

SECTION II. TASK 2. SUBMODEL DEVELOPMENT AND EVALUATION

Objectives

The objectives of this task are to develop or adapt advanced physics and chemistry submodels for the reactions of coal in an entrained-bed and a fixed-bed reactor and to validate the submodels by comparison with laboratory scale experiments.

Task Outline

The development of advanced submodels for the entrained-bed and fixed-bed reactor models will be organized into the following categories: a) Coal Chemistry (including coal pyrolysis chemistry, char formation, particle mass transfer, particle thermal properties, and particle physical behavior); b) Char Reaction Chemistry at high pressure; c) Secondary Reactions of Pyrolysis Products (including gas-phase cracking, soot formation, ignition, char burnout, sulfur capture, and tar/gas reactions); d) Ash Physics and Chemistry (including mineral characterization, evolution of volatile, molten and dry particle components, and ash fusion behavior); e) Large Coal Particle Effects (including temperature, composition, and pressure gradients and secondary reactions within the particle, and the physical effects of melting, agglomeration, bubble formation and bubble transport); f) Large Char Particle Effects (including oxidation); g) SO_x - NO_x Submodel Development (including the evolution and oxidation of sulfur and nitrogen species); and h) SO_x and NO_x Model Evaluation.

II.A. SUBTASK 2.a. - COAL TO CHAR CHEMISTRY SUBMODEL DEVELOPMENT AND EVALUATION

Senior Investigators - David G. Hamblen and Michael A. Serio
Advanced Fuel Research, Inc.
87 Church Street, East Hartford, CT 06108
(203) 528-9806

Objective

The objective of this subtask is to develop and evaluate, by comparison with laboratory experiments, an integrated and compatible submodel to describe the organic chemistry and physical changes occurring during the transformation from coal to char in coal conversion processes.

Accomplishments

Work continued on the improvements to the FG-DVC model. A set of rank dependent kinetic parameters has been developed for tar, CH₄, CO, H₂O, and CO₂ for each of the Argonne coals. The predictions of the model are being compared to pyrolysis kinetic data from the TG-FTIR system at four heating rates. The 2- σ percolation theory version of the model is currently being used to develop the kinetic parameters for the gaseous volatile species, since it has a much faster execution time than the Monte Carlo version. Since the gas evolutions are predicted by the FG part of the FG-DVC model, these are independent of the type of network decomposition calculations. For a given coal, it is being assumed that the pre-exponential factors are similar for the evolution of the components of a given species (e.g., CO₂-Extra Loose, CO₂-Loose, and CO₂-Tight), but that the activation energies increase in the order Loose ---> Tight. It is also being assumed that for a given species pool, the frequency factor is fixed (independent of rank) and that the activation energies for each functional group pool increase in the rank order. This approach has been successfully used for the component pools of the major volatile species (CO, CO₂, H₂O, CH₄) for four of the eight Argonne Premium coals, to date (Utah, Pittsburgh, Upper Freeport, Pocohontas). Work on the remaining coals is in progress.

Some of this work was summarized in a paper that will be presented at the ACS Washington Meeting (Serio et al., 1990). Additional work needs to be done

on refining the tar evolution kinetics for the two lowest rank coals (Zap, Wyodak) because of interferences from the polymethylene (PM) species which make the bridge breaking rates appear lower than they really are. For the low rank coals, experiments with demineralized coal are being used to elucidate the rates. In this case, the tar species are more important in contributing to the tar peak.

The kinetic parameters were tested in both Monte Carlo and the 2- σ percolation theory version of the FG-DVC model. Results for three of the eight coals indicate that only small adjustments are required in the model kinetic parameters between the two models. Of course, the network configuration parameters are inherently different. We will be doing a sensitivity analysis to see which parameters should be changed so that the two versions are as similar as possible.

The kinetic parameters are also being validated indirectly through the application of the fluidity model to the Geissler fluidity data for six of the eight Argonne coals. The fluidity predictions are strongly dependent on the kinetics of bridge breaking and crosslinking. In the FG-DVC model, crosslinking is tied to the evolution of CO₂ at low temperatures and CH₄ at high temperatures. Most of the recent adjustments have been in the kinetic parameters for CH₄-Loose and CH₄-Tight. Additional work has been done with the fluidity model.

Comparisons are also being made to the NMR data of Lynch obtained at CSIRO on the Argonne premium coals. The changes in the fluid fraction predicted from the fluidity model are in good agreement with the change in hydrogen mobility observed in the NMR experiment. We are rechecking the current version of the model with the latest kinetic parameters against van Krevelen's data for fluidity as a function of heating rate and against the isothermal data of Oxley and Pitt.

Work also continued on the swelling model. By using an adjustable parameter for either the diffusion distance or bubble wall thickness in the model, we were able to obtain good predictions for swelling ratio, porosity, and surface area over a range of pyrolysis heating rates. However, we are concerned by the absence of bubble rupture in the model, as the data obtained at Rice University suggest that this is an important phenomenon. We are supposed to receive some videotapes of the experiments done at Rice, and we plan to examine these before reformulating the model.

Determination of Kinetic Rates

Considerable effort has been made in the past three months in the attempt to determine the kinetic rate parameters for major devolatilization products in the Argonne coals based on the TG-FTIR and other available experimental data. During this process, attention has been paid to the rank variation of these kinetic parameters, as well as to the relationships between different volatile products.

For most gas evolution data, the measured rate curves often show several distinct peaks or peaks overlapping each other. This implies that more than one reaction is required to describe the gas evolution. In our FG-DVC model, we often use several different pools (such as CO₂ - Extra Loose, CO₂ - Loose, CO₂ - Tight) to describe a multiple evolution curve. Each pool is associated with its own rate constant including frequency factor A and activation energy E with a distribution σ . The rate expression has the form

$$K = A \exp (- (E \pm \sigma)/RT)$$

In addition to the three parameters, each pool has another parameter, namely a weight fraction to be determined. It is obvious that when there are so many parameters associated with a single gas specie, the goal of finding a unique solution based on the limited data is sometime impossible. The widely scattered kinetic data reported in literature are at least partially due to this difficulty.

In order to derive a set of kinetic rates reasonable for the major volatile products in the Argonne coals, we laid down the following guidelines to determine the kinetic parameters based on our understanding of the Arrhenius equation and the rank variation of coal kinetics. The experimental data used to determine these parameters include the TG-FTIR measurements at four different heating rates and some high heating rate data.

1. The Frequency Factor

The literature data show a great scatter in the frequency factor of coal pyrolysis, which ranges from the order of 10³/sec up to 10²⁰/sec. For gas phase

reactions, the frequency factor is conceptually understood as the number collisions of the reactants per unit time. For coal devolatilization products, the reactions are mainly the dissociation of functional groups from a coal macromolecular network which falls into the category of unimolecular reactions. The mechanism of these reactions is widely accepted as the following: when enough energy gets into a particular mode of vibration, the vibration of the molecule in this mode leads to dissociation of the molecule.

Although the theoretical calculation of the frequency factor for unimolecular dissociation is rather complex, it is reasonable to assume that the frequency factor of dissociation is comparable to the average vibrational frequency of a molecule which is known to be in the order of 10^{13} /sec for solids. Therefore, we propose an upper limit of the frequency factor to be 1×10^{15} /sec, taking into account the degree of uncertainty and some possible self-activated high frequency modes.

It is also known that the frequency factor could be weakly temperature dependent, as predicted by the collision theory to be proportional to T and by the theory of absolute reaction rates to be proportional to T (Castellan). The weak dependency is meant to be compared with the exponential dependency of temperature in the Arrhenius equation. Based on this reasoning, we allow some increase in the frequency factor with temperature, but not exceeding the proposed upper limit. For example, the CO_2 - Tight pool that evolves at higher temperature would have the frequency factor 7.5×10^{12} /sec, higher than 5.0×10^{12} /sec chosen for the CO_2 - Loose pool.

2. The Activation Energy

The activation energy is considered as the energy barrier that the reactants have to overcome to accomplish the reaction. The rule of thumb is that the higher the temperature at which a reaction takes place, the higher the activation energy the reaction is associated with.

The activation energy of a reaction (E) and its distribution (σ), together with its frequency factor (A), can be determined to a certain accuracy if the evolution rates and the corresponding peak temperatures of the reaction are measured accurately at several different heating rates. We have used the curve

fitting approach to determine the bond-breaking rate for eight Argonne coals based on the TG-FTIR measured tar evolution curves at different heating rates. Since the tar evolution is usually a single-peak curve, the above approach worked well.

However, for the multi-peak evolution curves, the determination of the kinetic parameters is more complicated. In addition to the above-mentioned guidelines for choosing the activation energy and the frequency factor, we have defined certain rules for rank variation and the relationships between the gas pools of different species.

3. Rank Dependency

When comparing the multi-peak evolution curves of a given specie in different coals, one would notice an interesting feature. As the coal is increased in rank, the leading edges and the early peaks (Extra Loose or Loose pools) shift to higher temperatures while the trailing edge (Tight or Extra Tight pools) remain at the same temperature. An example of this is shown for water for five coals in Fig. II.A-1 (Solomon et al., 1990b). From this figure it appears that this feature can be explained in the light of the geological aging process of coal formation. With increasing aging temperature and time, maturation process gradually evolves the loosely bounded functional groups and leaves the tightly bounded groups intact.

This feature also provides us with a guideline for the kinetic rates, namely, we keep the same frequency factor for the same pool. The activation energy of the pool then increases with increasing coal rank to fit the data. We find that the activation energy of tight pools generally change with rank much less than do the loose pools.

4. Relationships between Kinetic Rates of Different Volatile Species

It is found that some pools in the different gas species have peak evolution rates at the same temperature and those peaks have the same shifts when the heating rate changes. The Utah Blind Canyon coal gives a good example as shown in Fig. II.A-2. The TG-FTIR measurements indicate that the tar evolution, the CO₂-Loose, CO-Loose, and the H₂O-Loose pools all show very close peak

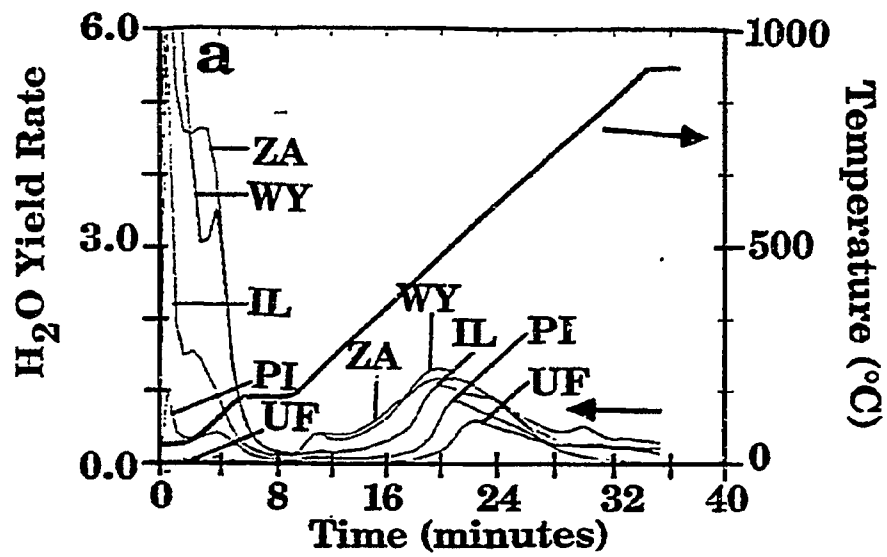


Figure IIA-1. Evolution Curves for H₂O Measured in a TG/Plus for Five Coals from the Argonne Premium Samples Collected at 30°C/min (UF-Upper Freeport, PI-Pittsburgh, IL-Illinois, WY-Wyodak, ZA-Zap Lignite).

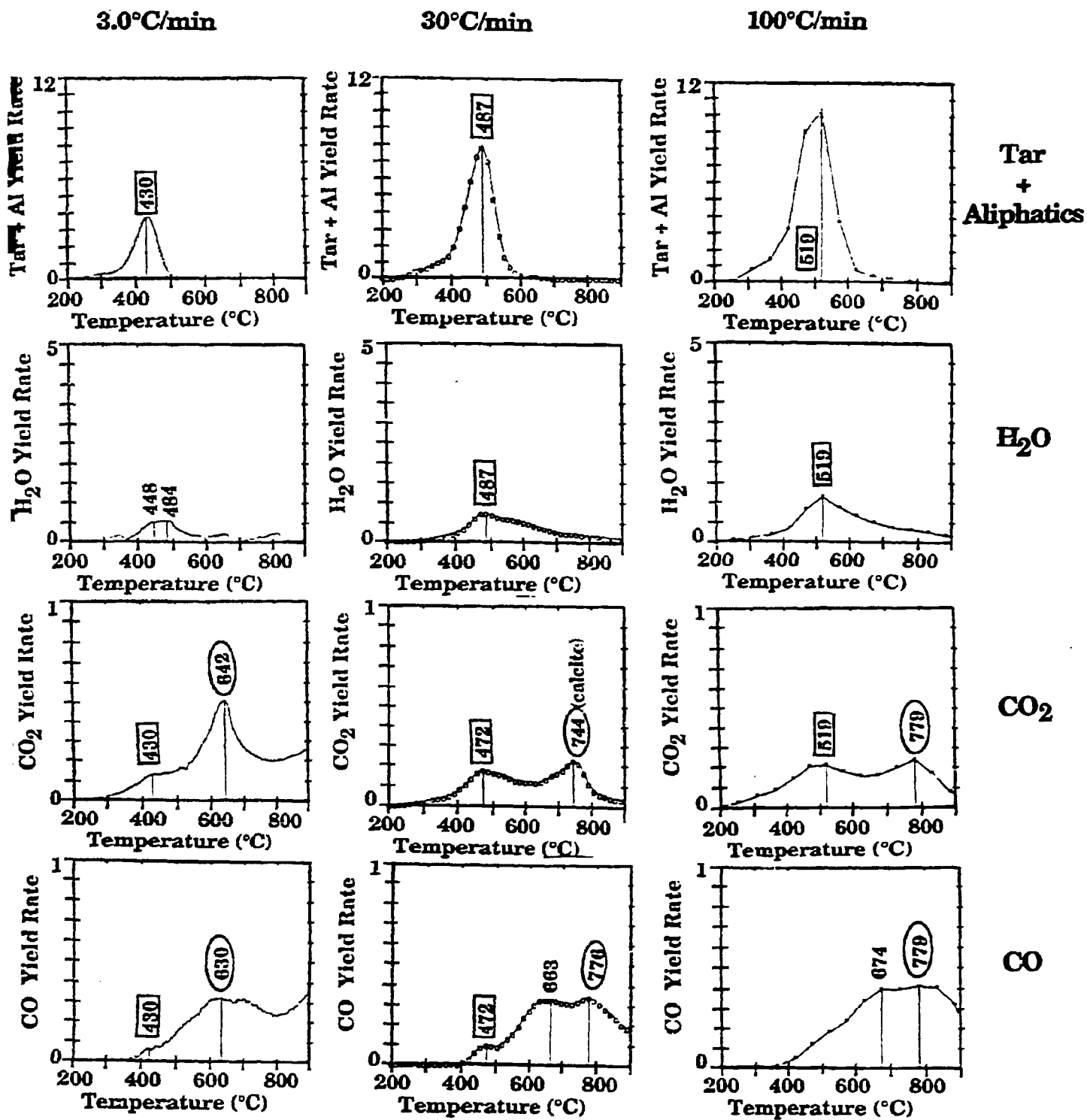


Figure IIA-2. Evolution of Tar, H₂O, CO₂, and CO from Utah Blind Canyon Coal at Three Heating Rates.

temperature at about 480°C for 30°C/min, at about 519°C for 100°C/min and at about 430°C for 3°C/min runs. This feature implies that these volatile pools can be fit with the same kinetic parameters. This may also imply that there is some common chemistry.

By using all the guidelines discussed so far, we were able to narrow down the range of choice for the kinetic parameters and determine a reasonable set of rank dependent kinetic rates for the Argonne Premium coals.

5. Results

A typical comparison of theory and TG-FTIR experiments is shown in Figs. II.A-3 to II.A-5 for three heating rates. The agreement between the theory and experiment is generally quite good except for CO₂. For this specie, residual oxygen in the reactor causes some oxidation at the slowest heating rate and minerals contribute evolved CO₂ which is not modeled. CO also shows some differences in the predicted amplitude, while the agreement is good for water, U-loss, CH₄, tar and H₂O.

We have applied these curve fitting procedures for the eight Argonne coals according to the rules cited above (i.e., frequency factor less than 10¹⁵/sec and constant for a seven gas species pool independent of coal rank). Preliminary results for the three CO pools are presented as a factor of the coals' oxygen concentration in Fig. II.A-6. As can be seen, there is a systematic increase in activation energy with increasing rank. The variation in activation energy is maximum for the loose pool and reduces as the activation energy increases.

As mentioned previously, the lowest rank coals exhibit tar evolution which does not follow the trend of decreasing peak temperature with decreasing rank. Data in Fig. II.A-7 shows the temperature for Wyodak coal tar is higher than that for Illinois No. 6 coal. The Wyodak tar is also substantially more aliphatic than is the Illinois No. 6, and it appears that the Wyodak tar is dominated by polymethylenes.

As discussed by Serio et al. (1990a), demineralization increases the tar yield. Results for the Wyodak subbituminous coal are presented in Fig. II.A-8. There is more tar for the demineralized coal. This tar is less influenced by

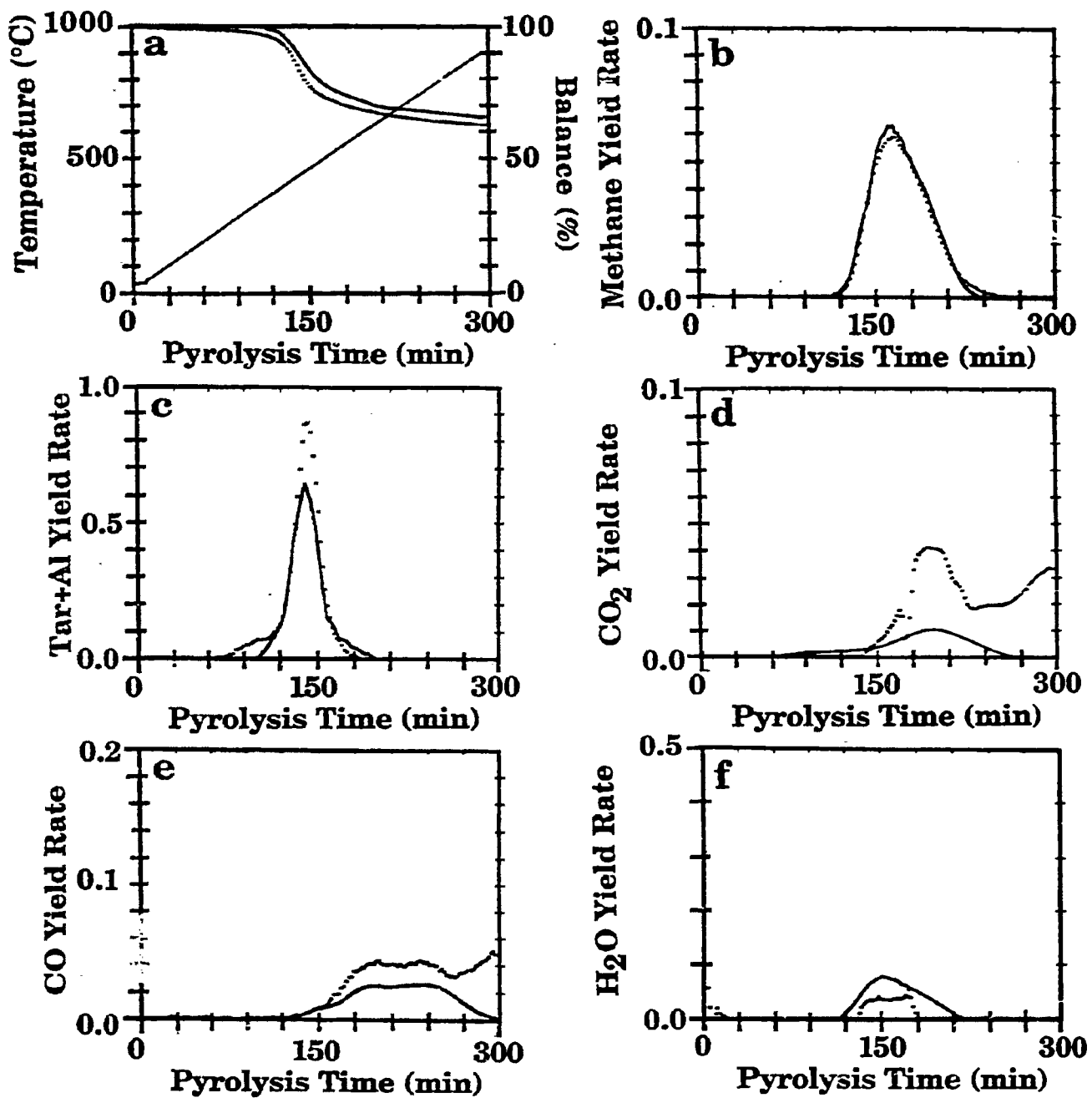


Figure ILA-3. Data from TG-FTIR Heating Rates (···) and Predictions of FG-DVC Model for Pittsburgh No. 8 Bituminous Coal at 3°C/min. a) Weight Loss and Temperature; b) Methane; c) Tar + Aliphatics Gases; d) CO₂; e) CO; f) H₂O.

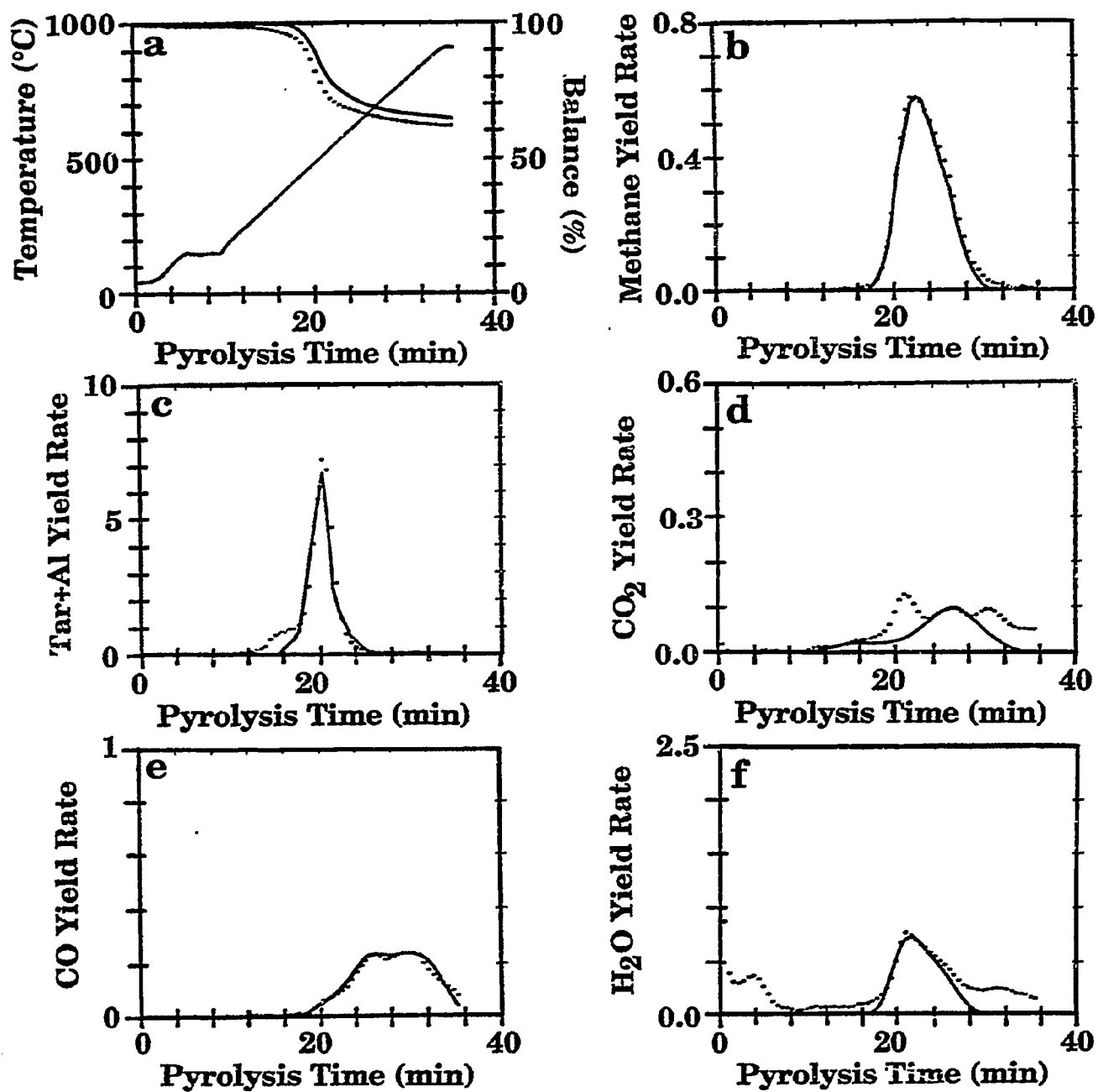


Figure IIA-4. Data from TG-FTIR Heating Rates (··) and Predictions of FG-DVC Model for Pittsburgh No. 8 Bituminous Coal at 30°C/min. a) Weight Loss and Temperature; b) Methane; c) Tar + Aliphatics Gases; d) CO₂; e) CO; f) H₂O.

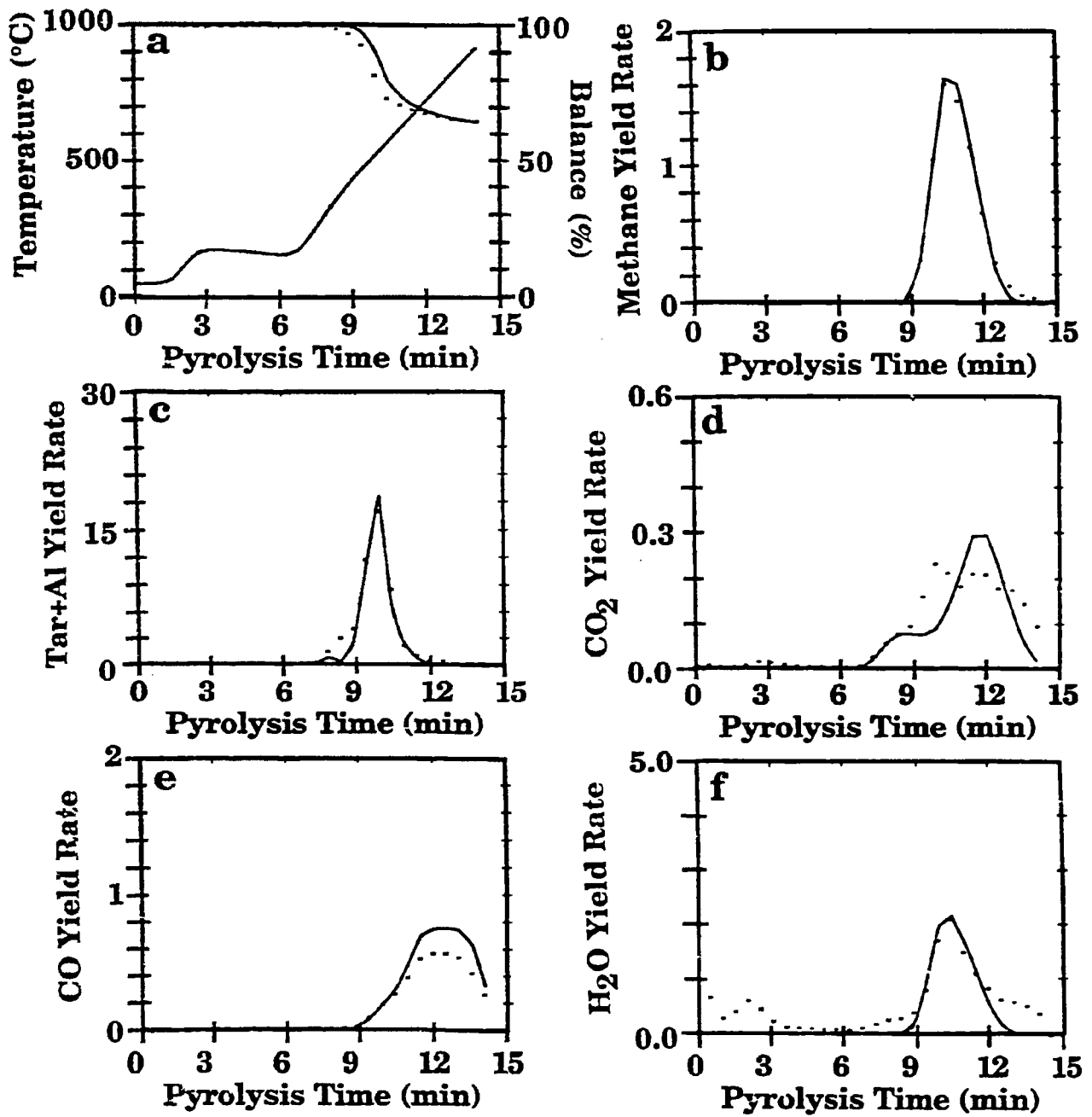


Figure IIA-5. Data from TG-FTIR Heating Rates (···) and Predictions of FG-DVC Model for Pittsburgh No. 8 Bituminous Coal at 100°C/min. a) Weight Loss and Temperature; b) Methane; c) Tar + Aliphatics Gases; d) CO₂; e) CO; f) H₂O.

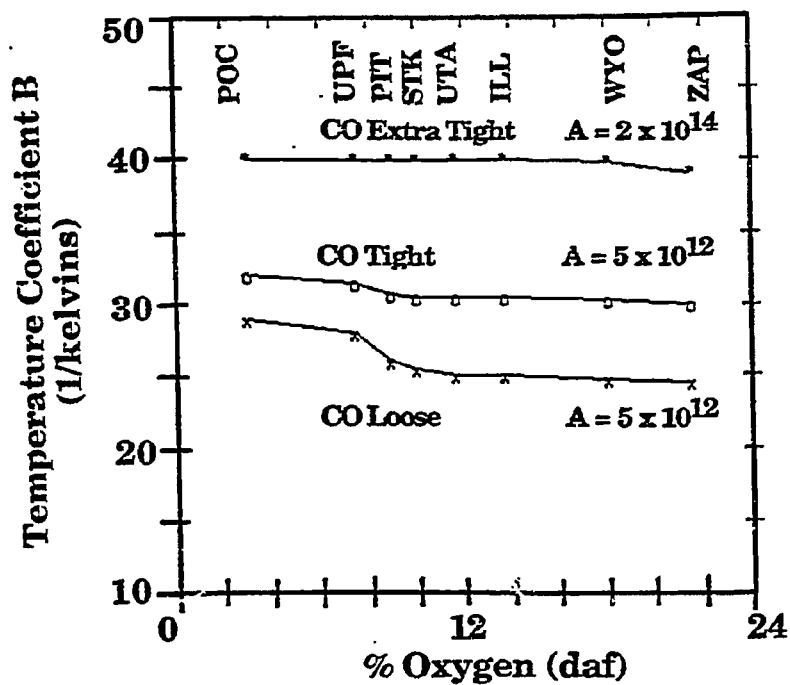


Figure IIA-6. Activation Energies for CO Loose, CO Tight and CO Extra Tight as a Function of the Coals Oxygen Concentration. The Frequency Factors are Shown in Parenthesis.

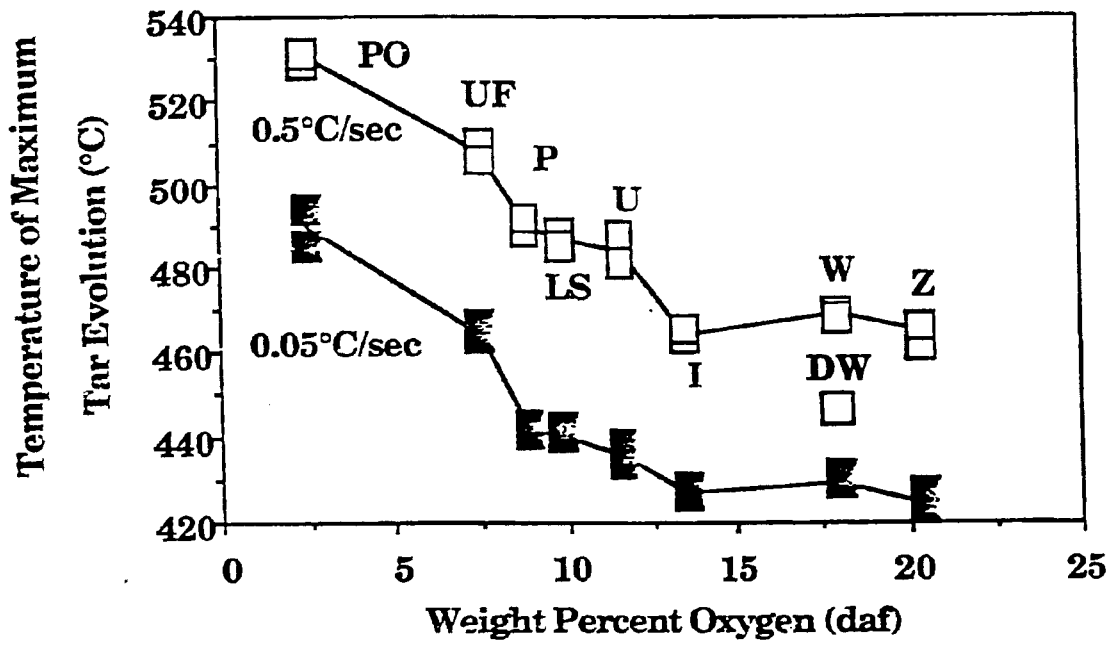


Figure ILA-7. Rank Variation of Tar Evolution Temperature.

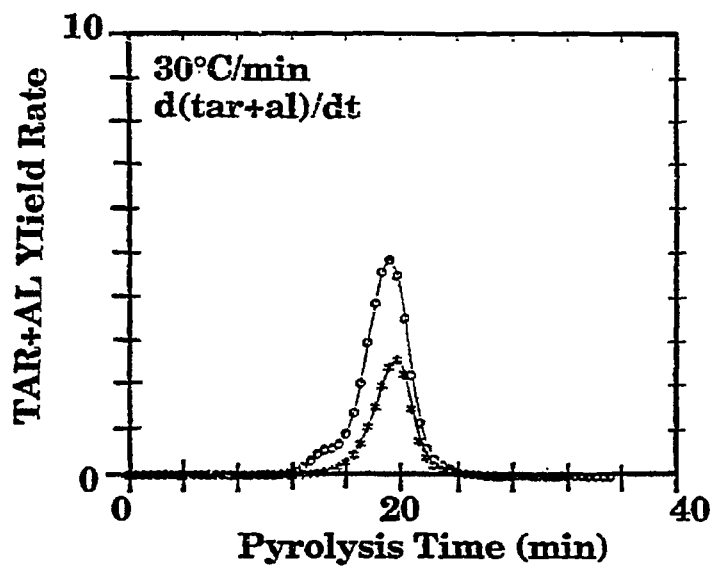


Figure IIA-8. TG-FTIR Analysis of Raw (*-*) and Demineralized (o-o) Wyodak Coal.

polymethylenes and the peak appears at a temperature about 20°C lower. The peak for the demineralized Wyodak (Markel DW) continues the trend for decreasing temperature with decreasing rank as shown in Fig. II.A-7.

Comparison of Monte Carlo and 2- σ Percolation Models

The prediction of the FG-DVC model using both the Monte Carlo and 2- σ percolation tests are being compared. It appears that the 2- σ percolation theory can give equivalent predictions to the Monte Carlo version. It is preferable to use the 2- σ percolation theory version because of its speed and lack of statistical variation. Figure II.A-9 presents a comparison of the two models for predicting the liquid fraction, the tar, and the fluidity. The prediction of tar is compared to the tar yield measured in the TG/Plus. The predictions of fluidity are compared to Geissler fluidity measurements (Solomon et al., 1990c). Both models give comparable predictions which are in good agreement with the data.

The liquid fraction predictions are different. This difference has to do with what is defined as liquid. In the Monte Carlo model, the three largest network fragments are defined as char and the rest liquids. For the 2- σ percolation model, all unattached fragments were defined as liquid. We will be examining the appropriate definition to use for the 2- σ percolation model during the following quarters.

The liquid fraction was compared to unpublished data of Sakurovs and Lynch (1990), using proton magnetic resonance thermal analysis (PMRTA). The technique discussed by Lynch et al. (1988, 1988a) and Barton and Lynch (1989) measures the fraction of "mobile" hydrogen, where the mobility depends on the molecule's ability to rotate. The "mobile" fraction is zero at low temperatures because the temperature keeps even non-covalently bonded molecules rigid. As the temperature increases and the coal becomes fluid, the mobile fraction starts to resemble the predicted liquid fraction. Both predicted and measured "mobile" fractions reach a peak at the same temperature and decline in a comparable fashion.

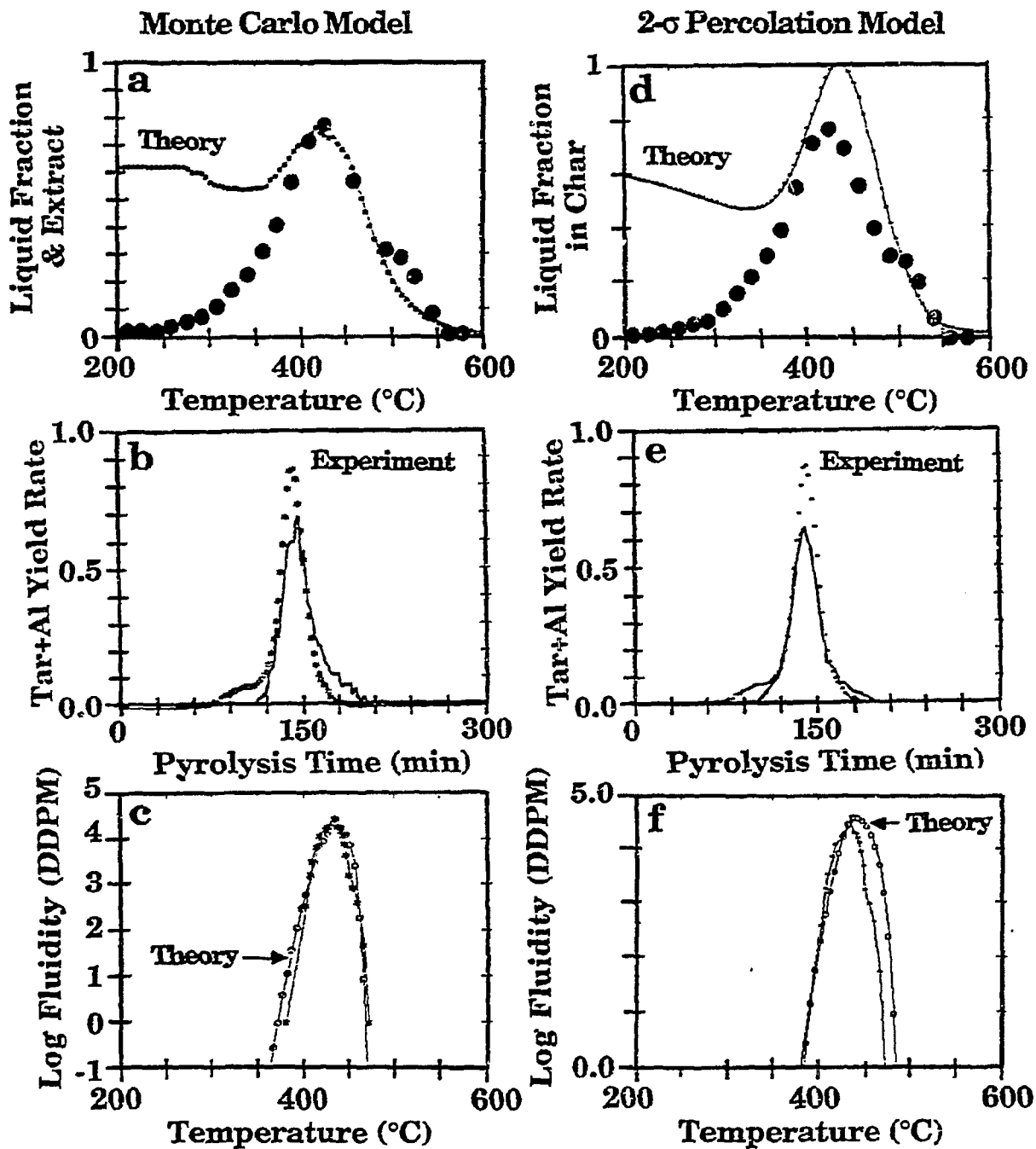


Figure IIA-9. Comparison of Monte Carlo and 2- σ Percolation Theory for Liquid Fraction, Tar Yield and Fluidity for Pittsburgh No. 8 Bituminous Coal at 3°C/min.

Plans

Determination of the rank dependent parameters will be completed and tested in the percolation theory version of the model by comparison to several data sets. In addition, the work on the swelling model will be continued. Work will be initiated on studying the evolution of sulfur and nitrogen species.

II.B. SUBTASK 2.B. - FUNDAMENTAL HIGH-PRESSURE REACTION RATE DATA

Senior Investigators - Geoffrey J. Germane and Angus U. Blackham
Brigham Young University
Provo, Utah 84602
(801) 378-2355 and 6536

Student Research Assistants - Charles R. Monson, Gary Pehrson,
David Wheeler, and James Rigby

Summary

During the last quarter significant progress in developing the optical particle imaging system and the reactor collection system was made. The optical stands and brackets were designed and fabricated for the HPCP facility. The time required for size classification of pulverized coal was considerably reduced and the quality of the classification was improved significantly. Sufficient quantities of narrow size ranges of two of the test coals were produced for upcoming char preparation and oxidation tests. Analytical techniques to determine tar composition directly from tar filters were also developed and improved accuracy of char weight loss analysis through the use of four simultaneous tracers was investigated. Previously collected char and tar from Pittsburgh No. 8 bituminous coal was analyzed and compared using the new procedures.

Objectives

The overall objective of this subtask is to measure and correlate reaction rate coefficients for pulverized-coal char particles as a function of char burnout in oxygen at high temperature and pressure.

Accomplishments

Three components of the subtask have been identified to accomplish the objectives outlined above: 1) develop the laminar-flow, high-pressure, controlled-profile (HPCP) reactor, 2) prepare char at high temperature and pressure, and 3) determine the kinetics of char-oxygen reactions at high pressure. The HPCP reactor, capable of functioning at 400 psi (27 atmospheres), has been constructed to perform the fundamental reaction rate measurements required for the study. Data from another char oxidation study

(atmospheric pressure) conducted at Brigham Young University will also be used.

Work continued during the last quarter on development of the optical particle imaging system and the reactor collection system. Significant progress was made in improving the size classification of pulverized coal and in reducing the time required. Sufficient quantities of narrow size ranges of two of the test coals were produced for upcoming char preparation and oxidation tests. Analytical techniques to determine tar composition directly from tar filters have been developed and improved accuracy of char analysis through the use of four simultaneous tracers has been investigated.

High Pressure Reactor Development and Characterization

Work during the reporting period has mainly focused on assembly of the optical instrument and improved size classification of pulverized test coals for char preparation and oxidation.

Optical Instrumentation - Mounting fixtures for all of the optical components as well as the laser, laser detector, and photomultiplier bases have been fabricated. A rotating pinhole wheel and mount was also fabricated for the calibration system. These fixtures provide sturdy mounting and easy adjustment for the instrument components. Alignment of the optics has begun as fixtures have been completed. Implementation of the optical instrument in the char oxidation experiments will improve the accuracy of the particle temperature history, resulting in more accurate reaction rate parameter determination.

The optical instrument is patterned after a system developed at Sandia National Laboratories for in situ measurement of single particle temperature, velocity and diameter (Tichenor et al., 1984). This system obtains temperature measurements by two-color pyrometry and particle velocity and diameter measurements through the use of an image-plane, coded-aperture technique. A new coded-aperture that improves diameter measurement accuracy, designed by Wells (1990), is also included in the optical instrument being assembled for this project. A description of the instrument and its operation follows.

Particle Imaging System - Figure II.B-1 is a schematic of the optical instrument. Incandescent particles moving along the centerline of the reactor

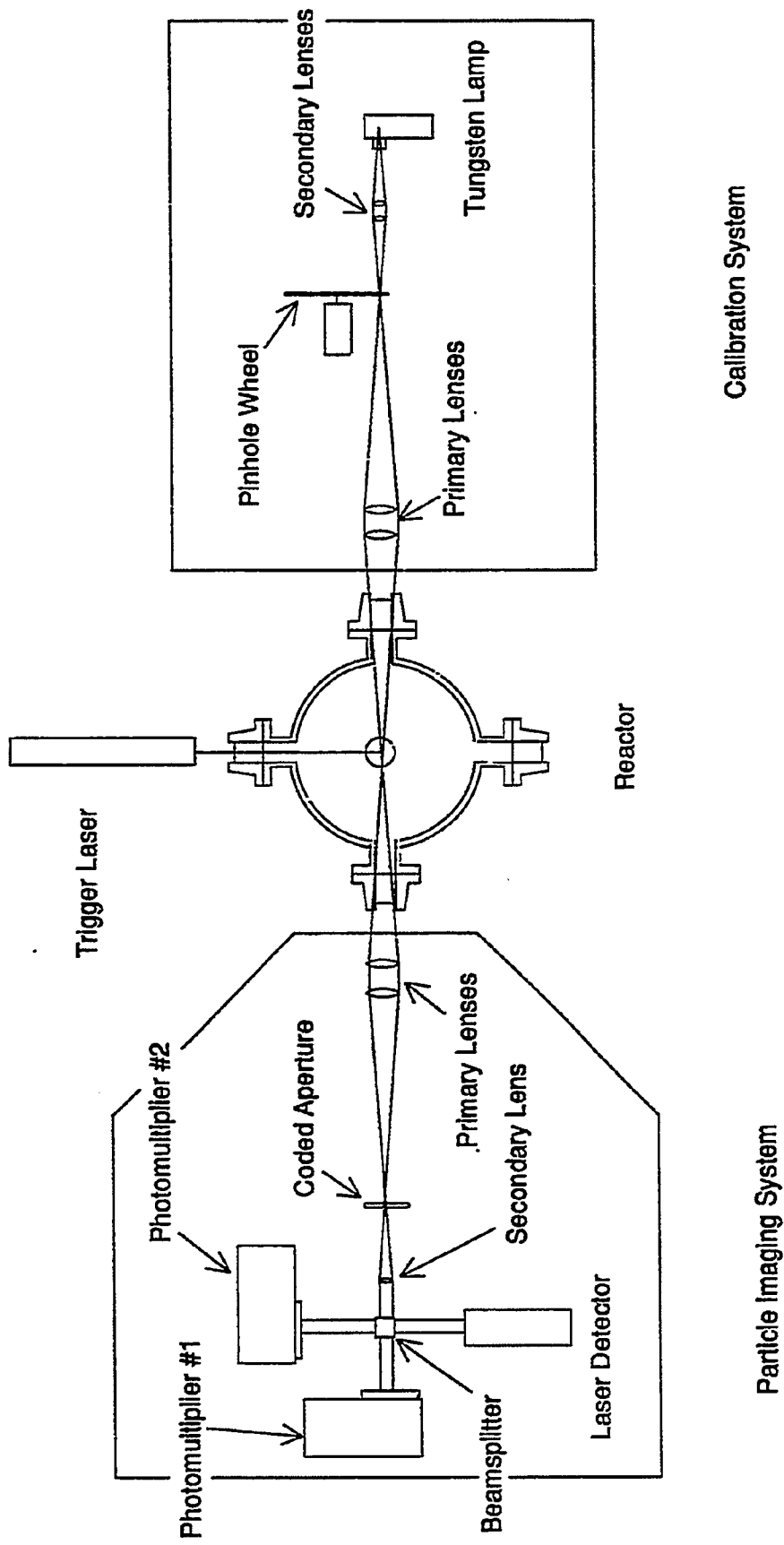


Figure II.B-1. Schematic of Optical Instrument

will be imaged at actual size onto a coded-aperture by a pair of lenses. The light transmitted through the aperture will be separated into two wavelength bands by a beamsplitter and two bandpass filters. The intensity of each of these wavelength bands will be detected by a photomultiplier tube and recorded by a high-speed digitizing oscilloscope. A laser beam, positioned perpendicular to the centerline of the optics immediately upstream of the sample volume, will act as a trigger. A particle moving down the centerline of the reactor will pass through the laser beam, scattering the laser light. A portion of this scattered light will travel through the optics to the laser detector. A pulse output from the laser detector will indicate that a particle is about to enter the sample volume and will trigger the oscilloscope to record the photomultiplier outputs. Because the laser is perpendicular to the optics centerline and directly above the optics focal point, only particles in focus will be measured. Specifications for the system components are listed in Table II.B-1.

The coded aperture with its dimensions is shown in Figure II.B-2. The upper-most slit provides passage of the scattered laser light that will be used for the trigger. This slit is much narrower than the others to ensure that only particles passing through the center of the optical volume will be sampled. Errors in particle diameter measurements would occur if the entire particle width is not visible through the wider slits. The large slit centered on the aperture is for temperature and velocity measurements. This slit is large enough to allow the entire particle to be visible for a short duration. The three blackouts that make up the lower portion of the aperture will be used to obtain particle diameter. As a particle passes behind a blackout, its signal will be attenuated, which occurs as a function of particle diameter.

Calibration System - A calibration system, also shown in Figure II.B-1, is built into the instrument to provide temperature, velocity and diameter standards as well as to determine the system gain constant. The calibration system will project a false particle image into the sample volume of the reactor. This image will be formed by focusing a tungsten strip lamp of known temperature onto a series of pinholes that are mounted on a disc rotating at a known speed. The pinholes (25, 50, 75, and 100 μm diameters) will chop the tungsten strip light beam and a pair of lenses will focus the false particle images into the sample volume.

Table II.B-1
Optical Instrument Component Specifications

Optics

Primary Lenses:	356 mm F.L.	$\frac{f}{5.6}$	Cemented Achromat
Secondary Lenses:	127 mm F.L.	$\frac{f}{5}$	Cemented Achromat
Beam Splitter:	35 mm x 35 mm		50% Transmission & Reflection
Filters:			

<u>Center wavelength (nm)</u>	<u>Bandwidth (nm)</u>	<u>Transmittance at CWL (%)</u>
400	40	54
700	40	58

Photomultiplier Tubes

Hamamatsu R928

(Quantum Efficiency: 20% @ 400 nm, 4% @ 700 nm,
thermoelectrically cooled to 250 K)

Trigger

5 mW HeNe Laser

Thorn EMI DA-603 Laser Detector

Data Acquisition

Nicolet 2090-3C 2 MHz Digital Oscilloscope

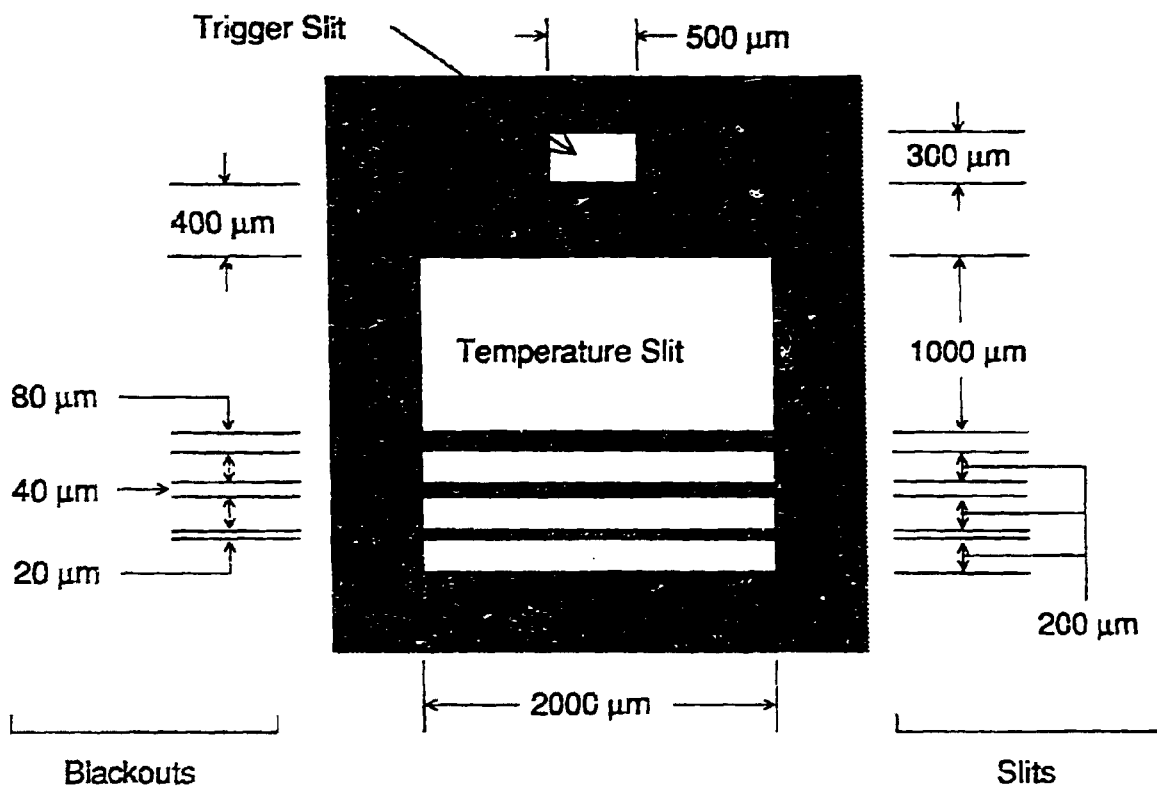


Figure II.B-2. Coded Aperture Configuration

Table II.B.2
Elemental Analysis of Char/Tar Sets

Sample		%C	%H	%O	H/C
P8-P-15	Char	72.0	3.2	2.6	0.044
P8-P-15	Tar	79.4	4.7	2.8	0.060
P8-P-19	Char	75.1	2.6	2.7	0.035
P8-P-19	Tar	80.2	3.8	2.9	0.047
P8-P-22	Char	76.5	0.8	2.5	0.010
P8-P-22	Tar	82.3	1.5	2.8	0.018

Temperature Determination - Particle temperature will be determined using the relative intensity of emitted radiation in the two wavelength bands. Using Planck's radiation law and assuming that the particles behave as gray body emitters, the temperature is related to the photomultiplier outputs by the following equation,

$$T = \frac{C_2(i_1 - i_2)}{i_1 i_2} \left[5 \ln \left(\frac{i_1}{i_2} \right) + \ln K \right]^{-1} \quad (\text{II.B-1})$$

where T is particle temperature, λ_1 is the center wavelength of channel #1, λ_2 is the center wavelength of channel #2, C_2 is the second thermal radiation constant, and K is the calibration gain constant.

Velocity Determination - The vertical component of particle velocity will be determined from the transit time of the particle through the temperature slit of the coded-aperture:

$$V = \frac{h}{t} \quad (\text{II.B-2})$$

where V is particle velocity, h is the aperture temperature slit height, and t is the particle transit time.

Diameter Determination - At a given wavelength and temperature, the intensity of emitted radiation from a particle is proportional to the projected particle area. Assuming a spherical particle, the particle image will be that of a full circle in the temperature slit of the coded-aperture. When the particle passes behind one of the blackouts, a smaller area will be visible. This can be used to determine the following relation between particle diameter and the relative intensity of particle emission when fully visible and when partially blocked. Because this is based on the assumption of a spherical particle, some error will be introduced with nonspherical particles. The size measurement is an indication of the particle height as follows:

$$\frac{S_b}{S_f} = \frac{2}{p} \arccos \left(\frac{a}{d} \right) - \frac{2a}{pd^2} \sqrt{d^2 - a^2} \quad (\text{II.B-3})$$

where d is the particle diameter, a is the aperture blackout height, S_b is the signal of a partially blocked particle, and S_f is the signal of fully visible particle.

Detection Limits - The minimum particle size and temperature that can be measured with the optical instrument will be limited by the shot noise in the system. With a system similar to the one being assembled for this project, Wells (1990) found that at a signal to noise ratio of 10, the temperature of a 30 μm particle could be detected at a temperature as low as 1100 K. At the same signal to noise ratio, while using the 20 μm blackout on the coded-aperture, the diameter of a 30 μm particle could be detected at a temperature as low as 1000 K.

Tar/Char/Gas Collection System - A new version of the collection and separation system was designed under a separately funded project during the reporting period. In the modified design, a sintered stainless steel tube extends from the entrance of the collection probe to the virtual impactor nozzle. Cold nitrogen passes through this tube, quenching reactions in the collection probe and reducing tar buildup on its inner surface. The modifications are intended to reduce tar buildup in the virtual impactor by considerably reducing the overall size of the impactor body.

Char Preparation at High Temperature and High Pressure

During the reporting period, emphasis has been given to decrease the particle size range of the fractions of the selected coals. Work has also continued on the analysis of the tar fractions from earlier char preparation runs with the Pittsburgh #8 coal. The tar fractions were collected on glass microfibre filters. The CHN analyses of these tar/filter samples has been attempted without removing the tar from the filter.

Coal/Char Size Classification - Previously, some of the coal samples appeared to have small particles adhering to the particles in the expected size range. Considerable reduction in the amount of these small particles has been achieved using a combination of sieving and aerodynamic classification. Therefore, samples of the selected coals are being fractionated by this procedure into the two size ranges for the oxidation kinetic runs. These narrow size fractions are being characterized by a Coulter Counter for

particle size distribution, and a scanning electron microscope for size and shape determination.

In addition to the North Dakota Lignite, Pitt #8 bituminous coal was also classified for testing. The same procedure of classification, sieving, and grinding was used as was described in the last quarterly progress report. However, because of the large initial size of the Pitt #8 sample, the coal was pulverized before being classified with the Vortec Classifier. Currently, the pulverizer produces coal particles with a mean diameter of 50 μm . A higher mean diameter is desired for future sizing runs in order to reduce the production of particles with diameters less than 39 μm . A larger mesh pulverizer screen is expected to produce a mean diameter of 75 μm .

The Coulter Counter has been primarily used for checking coal classification since there have not been many tests. The electrolytic solution for the Coulter Counter is now being produced at BYU. The resistive properties of the solution are slightly different than those of commercially prepared solutions and requires recalibration of the Coulter Counter. After recalibration, this solution is expected to work as well as commercial solutions while also being more cost-effective.

Char/Tar Analysis - A procedure to determine the elemental composition of the tar has been developed. The tar collected on the glass fiber filters is used to measure the H/C ratio of the tar. This ratio should be higher than for the corresponding char from that char/tar set. The procedure leaves the tar undisturbed on the filter, enabling analysis of all tar samples, not only those with heavy tar loading on the filters. The sample placed in the Leco CHN-800 contains the tar and the filter. The mass of the glass-fiber filter is tared out prior to the analysis. Thus, the only mass the instrument sees is that of the tar. The filter residue is ashed and doesn't affect analysis.

Three samples from the Pitt #8 char/tar sets are compared in Table II.B.2. The H/C ratio in each case increases for the tars. An effect of temperature, pressure or residence time can be seen as the H/C ratio steadily decreases as those three variables are increased. This indicates that the tars are being cracked after evolution from the char before they reach the quenched collection probe.

Kinetics of Char-Oxygen Reactions at High Pressure

Literature Review - In a recent set of papers by Fletcher (1989a, 1989b), the importance of particle temperature measurements is discussed. It is thought that the wide difference in reported kinetic parameters of coal chars can be attributed to errors in determining particle temperatures. The weight loss measurements are improved using multi-element tracers (titanium, silicon and aluminum) in addition to ash. It is noted that the use of titanium as a tracer yields data that monotonically increase, while the other three tracers produced results with some occasional low data points. However, simultaneous use of all four tracers generally gave narrower confidence limits than could be determined using three or fewer tracers.

Other Activities

The senior investigator received several visitors from the People's Republic of China during the reporting period to discuss the ongoing work in coal combustion and high pressure char oxidation. The research team continued participation in the char oxidation coordination activities at BYU in which resources and results from three independent char oxidation studies are shared.

Plans

During the next quarter the installation of the new collection probe and virtual impactor will be completed for coal devolatilization and char oxidation tests, under independent funding. Alignment of the optical instrument will be completed during the next reporting period. The instrument will also be completely enclosed in a light-tight cover that will attach to the HPCP reactor. Since any stray light introduced into the optical system drastically increases noise, this will improve the instrument accuracy and allow operation of the system with the room lights on.

Computer control of the reactor wall heaters will also be implemented during this same period. This will reduce temperature deviation and improve repeatability of reactor conditions in addition to improving ease of reactor operation.

Work will continue to carefully size coal particles prior to char preparation and oxidation. An experimental plan will be finalized for the remaining coals using a predictive reaction code to suggest test conditions. Char preparation and oxidation using at least three of the test coals for this study will be initiated under carefully controlled conditions in the HPCP reactor.

**II.C. SUBTASK 2.c. - SECONDARY REACTION OF PYROLYSIS PRODUCTS AND CHAR BURNOUT
SUBMODEL DEVELOPMENT AND EVALUATION**

Senior Investigator - James R. Markham and Michael A. Serio
Advanced Fuel Research, Inc.
87 Church Street, East Hartford, CT 06108
(203) 528-9806

Objective

The objective of this subtask is to develop and evaluate by comparison with laboratory experiments, an integrated and compatible submodel to describe the secondary reactions of volatile pyrolysis products and char burnout during coal conversion processes. Experiments on tar cracking, soot formation, tar/gas reactions, char burnout, and ignition will continue during Phase II to allow validation of submodels in Phase II.

Accomplishments

Additional work was done on the coal flame experiments in the TWR using the FT-IR Emission/ Transmission Tomography technique. Two cases have now been completed for the Montana Rosebud coal (low velocity and high velocity). A low velocity case for the Pittsburgh Seam coal is about 50% complete. A paper based on a comparison of the two velocities and the two coal types was prepared for the ACS Washington meeting (Solomon et al., 1990d).

Plans

Complete tomography measurements for the two different coals (Montana Rosebud subbituminous, Pittsburgh Seam bituminous). Do color maps for presentation of tomography data. Continue characterization of TWR geometry and interact with BYU on PCGC-2 simulations of this system.

II.D. SUBTASK 2.d. - ASH PHYSICS AND CHEMISTRY SUBMODEL

Senior Investigators - James Markham and Michael Serio
Advanced Fuel Research, Inc.
87 Church Street, East Hartford, CT 05108
(203) 528-9806

Objective

The objective of this task is to develop and validate, by comparison with laboratory experiments, an integrated and compatible submodel to describe the ash physics and chemistry during coal conversion processes. AFR will provide the submodel to BYU together with assistance for its implementation into the BYU PGGC-2 comprehensive code.

To accomplish the overall objective, the following specific objectives are: 1) to develop an understanding of the mineral matter phase transformations during ashing and slagging in coal conversion; 2) To investigate the catalytic effect of mineral matter on coal conversion processes. Data acquisition will be focused on: 1) design and implementation of an ash sample collection system; 2) developing methods for mineral characterization in ash particles; 3) developing methods for studying the catalytic effects of minerals on coal gasification.

Accomplishments

No work was scheduled.

Plans

Continue study of mineral effects on the reactivity of low and high rank coals. Resume analysis of material and element balances from ash collections in the entrained flow reactor.

II.E. SUBTASK 2.e. - LARGE PARTICLE SUBMODELS

Senior Investigator - Michael A. Serio
Advanced Fuel Research, Inc.
87 Church Street
East Hartford, CT 06108
(203) 528-9806

Objective

The objectives of this task are to develop or adapt advanced physics and chemistry submodels for the reactions of "large" coal particles (i.e., particles with significant heat and/or mass transport limitations) and to validate the submodels by comparison with laboratory scale experiments. The result will be coal chemistry and physics submodels which can be integrated into the fixed-bed (or moving-bed) gasifier code to be developed by BYU in Subtask 3.b. Consequently, this task will be closely coordinated with Subtask 3.b.

Accomplishments

The work on the AFR fixed-bed reactor (FBR) system continued. No additional experiments were done during the past quarter. We are still evaluating the data which has been taken for the two stage experiments and the variable bed depths. A redesign of the experiment has been proposed and approved which will allow better quantitation of the tar yields and independent control of the temperature of the second bed. Assembly has begun on a redesign of the experiment.

Samples of large particles for each of the eight premium coals have been ordered from Argonne and should be received by July 1, 1990.

Discussions continued with BYU about the single particle FG-DVC model for use in the fixed bed reactor. For this purpose, AFR is developing an ordinary differential equation (ODE) version of the 2- σ percolation FG-DVC model. Additional refinements were done to the model. The speed has been increased so that it is now only four times slower than the standard percolation theory version. However, it is still two times faster than the standard Monte Carlo version.

The code was sent to BYU for integration into the Advanced Fixed-Bed Model. Further refinements were done of the ODE/percolation version of the FG-DVC model by using a different technique for integration of the activation energy distribution. This change affords an additional increase in the execution speed of a factor of five. This change can also be incorporated into other versions of the model. Discussions continued with BYU about the single particle FG-DVC model. A meeting was scheduled at AFR to discuss the single particle model which will involve members of both teams.

Differential Equation (ODE) Version of the 2- σ Percolation Model

During the current quarter, we have developed a version of the FG-DVC model which can be solved using a standard solver for ordinary differential equations (ODE). The solver used is the Livermore Solver of Ordinary Differential Equations with Sparse jacobian (LSODES). Previously, we had solved the equations with a combination of analytic solutions, where known, and Newton's method. We had used the assumption that the temperature was constant over a time step so that many of the equations could be solved analytically, and we used a suitably small time step to treat cases where the temperature was changing. For integration with the Fixed Bed modelling of Task 3, we needed to treat variable time-temperature behaviors in a more general manner; so the FG-DVC equations were cast into a form suitable for the LSODES code. The details of the equations are described in the attached Appendix A.

The model is identical in concept to that described in the general model paper (Solomon et al., 1988) and the network paper (Solomon et al., 1990e) except for a change made in the treatment of the distributed activation energy model (DAEM) of the kinetic rates. In the old versions, the assumption is that the starting distribution of activation energies, E_i , is assumed to be a truncated gaussian, and is simulated using 21 subpools, each of which is evolved over time and temperature. This means that after a short time, these distributions are no longer gaussian. Since the low energy subpools in the distribution evolve much faster (exponentially) than the higher energy pools, we were led in the new version to keep the distribution as a truncated gaussian, but to evolve the low energy truncation point with time. The validity of this assumption is supported by Figure II.E-1, which shows the evolution of the shape of the distribution in the original version of the model for several pools as

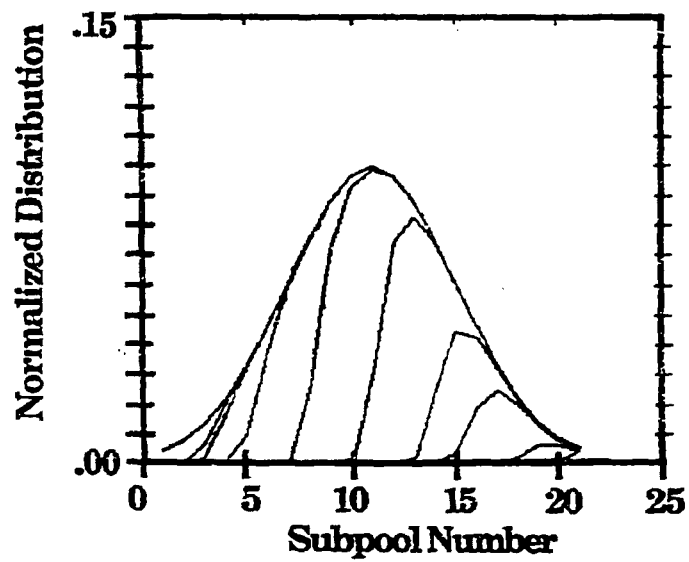


Figure ILE-1. Shape of the Species Source Distribution Function as it is Depleted (CO_2 extra loose at $30^\circ\text{C}/\text{min}$).

a function of time. The improved version would have a vertical line for the leading edge of the pool and is thus a reasonable approximation of the shapes in Fig. II.E-1. The benefit is of course that we have replaced 21 ODE's with a single one, for each of 27 functional groups.

The cpu run time in seconds for several cases run on a SUN 3/50 with a 68881 floating point chip is shown below:

Case	Improved ODE	ODE Version (7 subpools)	Standard 2- σ Percolation (21 subpools)	Monte Carlo FG-DVC (high rank coal)	Monte Carlo FG-DVC (low rank coal)
1	105 sec	500 sec	25 sec	180 sec	1600 sec
2	126 sec	619 sec	25 sec	180 sec	1600 sec
3	129 sec	632 sec	25 sec	180 sec	1600 sec
4	112 sec	287 sec	25 sec	180 sec	1600 sec

Case 1 is the slow heating rate (3°C/min) simulation of the TG-Plus (no tar cracking).

Case 2 is the regular heating rate (30°C/min) simulation of the TG-Plus (no tar cracking).

Case 3 is the fast heating rate (100°C/min) simulation of the TG-Plus (no tar cracking).

Case 4 is the slow heating rate (3°C/s) simulation of the viscosity measurement (with tar cracking).

The predicted gas and tar evolutions using the improved ODE version look identical to the original prediction using 21 subpools with a minimum adjustment of the activation energies (3% reduction).

Plans

Complete redesign of fixed-bed reactor system. Complete initial set of experiments on secondary reaction effects in thick beds. Continue development of single particle model with BYU and send the complete ODE version to BYU. Begin work on tar repolymerization model.

II.F. SUBTASK 2.F. - LARGE PARTICLE OXIDATION AT HIGH PRESSURES

Senior Investigators: Angus U. Blackham and Geoffrey J. Germane
Brigham Young University
Provo, Utah 84602
(801) 378-2355 and 6536

Student Research Assistants: Gary Pehrson and Michael Scheetz

Objectives

The overall objective for this subtask is to provide data for the reaction rates of large char particles of interest to fixed-bed coal gasification systems operating at pressure. The specific objectives for this quarter include selecting an additional individual for work on this study, reviewing more extensively the literature on the use of force transducers in high-pressure, high-temperature thermobalances, continuing discussion and evaluation of equipment design features, continuing evaluation of analytical procedures for monitoring the kinetics of oxidation of large particles, and conducting additional preliminary oxidation experiments.

Accomplishments

Two components of this subtask to accomplish the overall objective have been suggested in the plans outlined earlier: 1) high-pressure, large-particle reactor design, fabrication and preliminary data; 2) experimental reaction rate data for chars from five coals. The general features of the experimental unit will be a "large particle insert" to be placed in the HPCP facility of Subtask 2b. The "large particle insert" will consist of: (a) the reactor tube, (b) the balance unit, and (c) the connecting pipe. In this quarter, attention has been given to the development of the balance unit. A force transducer with specifications to permit monitoring of weight loss of 1-5 gram particles has been selected and ordered. An individual in the mechanical engineering program has been selected to work on the specific details of the design of the balance unit while experimental testing of the force transducer at atmospheric pressure is proceeding. Familiarity with the system at atmospheric pressure will help in anticipating difficulties when the balance unit is placed under pressure. A more extensive review of the literature on the use of force transducers in high-pressure, high-temperature thermobalances has been accomplished.

The testing of the new, single column for the gas chromatographic analysis of carbon monoxide and carbon dioxide was temporarily postponed during this quarter and will be accomplished during this next quarter.

An additional set of large particles of a Utah bituminous coal have been oxidized in platinum crucibles and compared with the results reported in the 14th Quarterly (Solomon, 1990).

High-Pressure, Large-Particle Reactor Design

Introduction and Literature Survey - The earlier review of the literature on thermobalances operating at high pressures was more concerned with use in coal combustion and gasification. Extension of this literature survey to the use of thermobalances in other types of chemical reactions has given additional information for the design of the experimental unit for this subtask.

Bae (1972) describes a simple thermogravimetric apparatus which was used at pressures up to 70 atm. The device was dumbbell-shaped with the furnace at one end and the balance unit at the other. A microforce transducer is used as the weighing device with an accompanying transducer amplifier-indicator to report and record the output. The maximum sensitivity of the transducer was approximately ± 0.1 mg. Satisfactory weight-loss thermograms were reported for the oxidation (with air) and evaporation of crude oil at temperatures up to 600° C and at pressures up to 70 atm.

Williams and Wendlandt (1973) reported the use of a high pressure thermobalance to study thermogravimetric curves of $\text{BaBr}_2 \cdot 2\text{H}_2\text{O}$, $\text{CuSO}_4 \cdot 5\text{H}_2\text{O}$ and NaHCO_3 at different pressures of nitrogen and/or carbon dioxide. The thermobalance was constructed by placing a DuPont Model 950 balance into a stainless steel enclosure. Maximum operating conditions were 500 atm (N_2) and 500°C. A change in sample mass due to a gas buoyancy effect as the pressure increased was easily corrected.

Dobner et al. (1976) discussed a high pressure thermobalance with maximum operating capabilities of 30 atm, 1100°C, with corrosive atmospheres and steam partial pressures up to 20 atm. A modified DuPont 950 TG was encased in a stainless steel pressure vessel. This modification of the TG was necessary to avoid damage by corrosive gases or steam. The reactions studied

were the cyclic CO₂-acceptor reaction for half-calcinated dolomite and the cyclic H₂S absorption and regeneration reaction for half-calcinated dolomite. Two problems were associated with this system. First, at 1 atm the baseline weight continuously increased with temperature at a rate of ~ 0.07 mg/100°C. Second, the baseline weight increased with total gas flow rate at a rate of ~0.08 mg/100 ml at 25°C and ~0.19 mg/ 100 ml at 925°C. These effects were caused by aerodynamic drag forces exerted by reacting gases flowing over the sample pan.

Li and Rogan (1978) reported the construction of a thermogravimetric system for corrosive environments at high pressures and temperatures. The reactor had a DuPont 951 thermogravimetric analyzer encased in a stainless steel high-pressure vessel. The maximum operating conditions were 60 atm and 1100°C with corrosive gases. Thermogravimetric studies were performed on the calcination of dolomite in CO₂/N₂ atm and the sulfidation of dolomite in H₂S/N₂ gas mixtures. A serious problem with this system concerns the initial transient readings of either sample temperature or gas composition.

Ghodsi et al (1979) describe a pressurized thermobalance featuring two symmetrical pans. The use of two symmetrical pans avoids thermogravimetric errors under pressure such as Archimedes' forces, viscosity forces and thermal gradient forces. A Sartorius 4406 thermobalance was modified for use at pressures up to 50 atm of H₂ and temperatures reaching 1000°C. The balance was tested using the hydrogenation of a lignite char as a preliminary application.

Forgac and Angus (1979) constructed a pressure chamber which held a Perkin-Elmer AM-1 autobalance within the walls. The sample is suspended in the hot zone with a wire (15cm length) made from nichrome, platinum and iridium. Sample holders were cylindrical crucibles made from 0.025 mm platinum foil. The thermobalance was run as a static system but is capable of dynamic flow. Experiments were done at temperatures of 1633 K and 70 atm. Although the design calculations allow for 2000 K and 136 atm.

Treptau and Miller (1987) describe a novel thermobalance. The reactor is internally heated and the entire reactor is weighed on a Mettler PE-360 top-loading electronic balance with a capacity of 60 ±0.001 g. The solid sample can be a fixed or fluidized bed through which reactant gas can flow. Gasification tests with CO₂ and O₂ were performed on coconut charcoal samples.

Experimental samples were 970° C and 600 psi with a balance sensitivity of ± 10 mg for a 2 g sample. The purpose of weighing the entire reactor was to provide direct measurement of sample temperature and elimination of external mass-transfer resistances via gas flowing through the sample bed. Nevertheless, a large scale drift on the balance of 0.1-0.5 g/hr was noticed when the gas flow rate was changed or pressure was increased during heating of the sample.

Experimental Approach - Analytical - It was indicated in the previous quarterly report (Solomon et al., 1990) that a new gas chromatographic column for simultaneous CO and CO₂ would be evaluated. The testing of this new column was temporarily postponed. However, this evaluation will be made soon and reported in the next quarterly.

Additional analyses have been made on coal, char and tar samples of coals to be used in this subtask. These analyses include CHN analyses with the LICO-CHN-800 instrument and Ti analyses with an ICP instrument. These procedures are ready for the analyses needed for this subtask.

The equipment for preparing sections of char and ash imbedded in epoxy resin has been received. Although this equipment is funded by another project, its availability for use in preparing samples for this subtask has been established. The necessary resins have been ordered so that thin section samples can be prepared from the preliminary large-particle oxidation runs and examined with the scanning electron microscope.

Experimental Reaction Rate Data

Preliminary Large Particle Oxidation Measurements - A set of large particles of a Utah bituminous coal was oxidized in platinum crucibles and the results reported in the 14th Quarterly Report (Solomon, 1990a). A similar set of particles of the same coal has been oxidized this quarter in platinum crucibles but in a small muffle furnace instead of with Mekker burners.

The results are presented in Table II. F-1. Six samples ranging in mass from 0.6 to 1.2 grams were first devolatilized in the flame of a Mekker burner so the flame would burn the volatile material. Samples were then placed in a muffle furnace for the oxidation of the char. The mass reactivity value of about 0.2 min⁻¹ reflects the mass loss during devolatilization. The overall average of 0.036 min⁻¹ is less than the value reported previously (0.046 min⁻¹).

TABLE II. F - 1

PRELIMINARY LARGE PARTICLE OXIDATION MEASUREMENTS

Coal: Utah Bituminous

Temperature: approximately 1230 K

Conditions: Oxidation in Air with Platinum Crucibles and a Muffle Furnace

Crucible# 1	#2	#3	#4	#5	#6	
Mass of Sample (grams)	1.048	0.781	1.184	0.0697	0.645	0.774
%Volatiles	46.1	43.9	44.2	37.6	34.1	39.5
%Ash	7.9	6.5	7.5	7.0	10.5	6.6
Mass Reactivity (Minutes ⁻¹)						
Time (minutes)						
2.0	.23	.22	.22	.19	.17	.20
7.0			.026	.024	.033	.024
12.0	.029	.032	.032	.043	.038	.036
17.0	.038	.044	.025	.041	.047	.036
22.0	.026	.037	.028	.036	.046	.046
32.0	.032	.046	.025	.043	.043	.037
47.0	.033	.029	.026	.034	.016	.039
62.0	.005		.036		.002	
82.0	.003		.007			
Average (except first and last values)	.0316	.0398	.0283	.0374	.0414	.0363

Overall average 0.0358

1). However, the temperature in these runs has a higher value. Both temperatures, however, are approximate and measured in different ways. The thermocouple junction of the muffle furnace is in back of the furnace half way up. The crucibles were positioned two at a time in the front of the furnace box with the door just slightly opened. Therefore, the temperature is probably less than the 1240 K and would appear to be also less than 1150 K reported previously. This shows the usefulness of making preliminary measurements to help anticipate the problems that may arise later. The ash values were less in the earlier measurements. The reason for this is not readily apparent.

Plans

During the next quarter the force transducer will be tested in a balance unit to be operated at atmospheric pressure. With this simple unit the characteristics of the force transducer in monitoring weight loss of coal samples at atmospheric pressure will be determined. The details of the balance unit for operation at high pressures will be included in the design of the "large particle insert." Machining of certain parts of the large particle insert will start.

Evaluation of the new gas chromatographic column will continue. Samples of char and ash imbedded in resin will be prepared and examined with the SEM equipment.

Preliminary measurements of large particle oxidation will continue.

II.G. SUBTASK 2.G. - SO_x/NO_x SUBMODEL DEVELOPMENT

Senior Investigators: L. Douglas Smoot and B. Scott Brewster
Brigham Young University
Provo, Utah 84602
(801) 378-4326 and (801) 378-6240

Research Assistant: Richard D. Boardman

Objectives

The objectives of this subtask are 1) to extend an existing pollutant submodel in PCGC-2 for predicting NO_x formation and destruction to include thermal NO, 2) to extend the submodel to include SO_x reactions and SO_x-sorbent reactions (effects of SO₃ nonequilibrium in the gas phase will be considered), and 3) to consider the effects of fuel-rich conditions and high-pressure on sulfur and nitrogen chemistry in pulverized-fuel systems.

Accomplishments

Predictions for coal combustion and gasification cases have been completed to verify the extended and alternative fuel NO mechanisms of the NO model. The ability to predict NO formation during gasification of North Dakota lignite was given special consideration. Joint fuel and thermal NO predictions were also completed for combustion and gasification cases. Some of the cases that were evaluated will be discussed in this report.

The revised NO model has been fully integrated into PCGC-2 and a user's guideline has been prepared (Boardman, 1990). Work is in progress to complete a sorbent reactions submodel. There are three main components associated with this subtask; 1) modification of PCGC-2 to track reactive sorbent particles, 2) incorporation of a sorbent reaction chemical model into PCGC-2, and 3) evaluation of the model by comparing predictions to experimental data. A brief discussion on this work will also be given in this report.

NO_x Submodel Development

Fuel NO Mechanisms Evaluation - A discussion about the improvements and revisions that were made to the existing NO model of Hill et al, (1984) was

given in the 3rd Annual Report (Solomon et al., 1990). In summary, a pathway for coal nitrogen to be released as NH₃ and an alternative fuel NO mechanism framework which includes NH₃ as a key intermediate were incorporated into the model (see Figure II.G-1). The improved NO model is generalized to allow the global kinetics reported by de Soëte (1975), Mitchell and Tarbell (1982) or Wendt and coworkers (Bose et al., 1988) to be used for predicting homogeneous formation and destruction of HCN, NH₃ and NO. Table II.G-1 lists the alternative kinetic rate expressions used in the revised NO model.

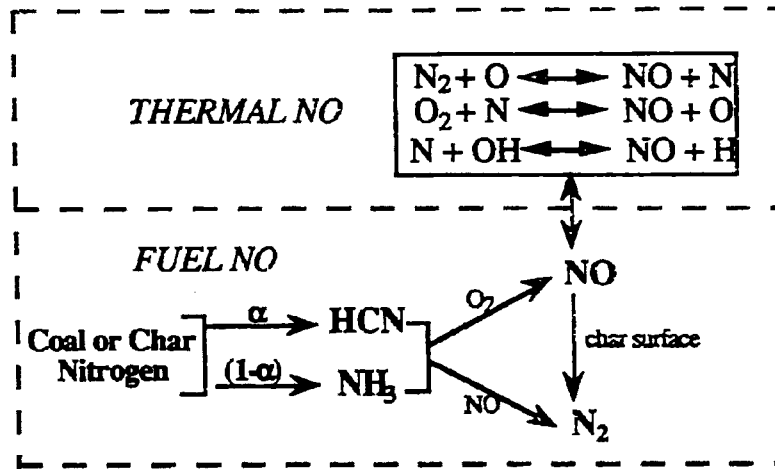
Pulverized Coal Combustion Comparisons - Coal combustion cases that were previously predicted by Hill et al. (1984) and Boardman and Smoot (1988) were re-evaluated using the revised NO model to examine revisions in the model. Only the results for a Wyoming subbituminous coal combustion case simulation will be discussed in this report. The burnout plot shown in Figure II.G-2 suggests that governing the flame structure is reasonably predicted for this case.

Figure II.G-3 compares the measured nitrogen-containing pollutant data with the profiles predicted using the global kinetics of de Soëte (1975). Excellent agreement is shown between the measured and predicted axial integrated profiles using a pre-exponential factor of 3.5×10^{10} for the global rate equation describing HCN oxidation to NO. The reported value of 10^{10} (de Soëte, 1975) underpredicts NO formation. The value of 3.5×10^{10} is within the range of experimental variability (de Soëte, 1986) and was determined to best fit several coal combustion and gasification cases. Therefore, it is recommended for predicting fuel NO when de Soëte's global kinetics are chosen to predict NO formation.

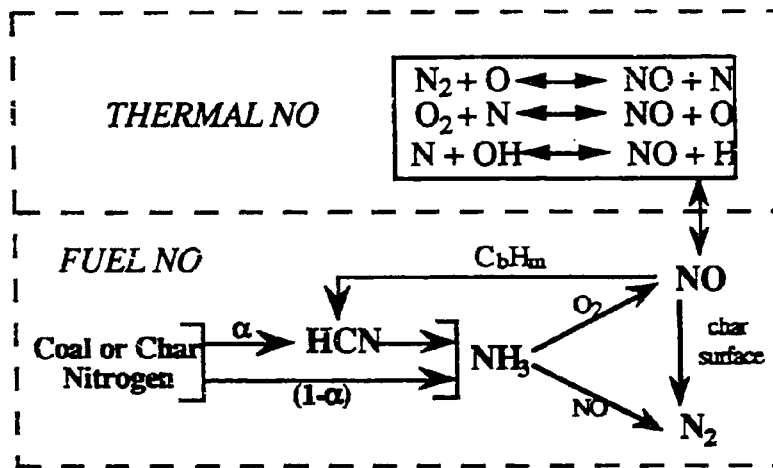
Mitchell and Tarbell (1982) give the only set of global kinetics which accounts for NO destruction by fuel fragments (CH_i's). The expression used to describe "reburning" reactions is:

$$\frac{dX_{NO}}{dt} = (10,000)X_{NO}X_{C_mH_n} \quad s^{-1} \quad (II.G-1)$$

The major limitation to using this expression is predicting the local concentration and molecular formula of fuel fragments, C_mH_n. An exact approach for predicting unreacted hydrocarbon concentrations would require using comprehensive reaction kinetics to predict the fuel oxidation process.



a. Extended fuel NO mechanism for the global kinetics of de Soëte (1975)



b. Alternative fuel NO mechanism for the kinetics of Mitchell and Tarbell (1982) and Wendt and coworkers (Bose et al., 1988).

Fig. II.G-1. Generalized mechanisms incorporated into the revised NO model of PCGC-2 for joint or separate prediction of fuel and thermal NO. Thermal NO is predicted by the Zel'dovich mechanism. Fuel NO is predicted using any of the optional fuel NO kinetics listed.

Table II.G-1
Reaction Expression Alternatives for the Revised NO Model.

Thermal NO Mechanism Reactions [‡]				
$k = A T^b \exp(-E/RT)$ (cm ³ gmole ⁻¹ s ⁻¹)				
Reaction Expression	Concentration	A	b	E (cal/gmole)
O + N ₂ → NO + N	X _{N₂} X _O	1.36x10 ¹⁴	0	75,500
N + NO → N ₂ + O	X _{NO} X _N	3.27x10 ¹²	0.300	-
N + O ₂ → NO + O	X _{O₂} X _N	6.40x10 ⁹	1.000	6,280
O + NO → O ₂ + N	X _{NO} X _O	1.50x10 ⁹	1.000	38,750
N + OH → NO + H	X _{OH} X _N	3.80x10 ¹³	0	-
H + NO → OH + N	X _{NO} X _H	2.00x10 ¹⁴	0	47,000

Fuel NO Mechanism Reactions				
$k = A \exp(-E/RT)$ (cm ³ gmole ⁻¹ s ⁻¹)				
Reaction Expression	Reference [§]	Concentration	A	E (cal/gmole)
HCN → NO	de Soëte (1975)	X _{HCN} X ^b _{O₂}	3.50x10 ¹⁰	67,000
HCN → N ₂	de Soëte (1975)	X _{HCN} X _{NO}	3.00x10 ¹²	60,000
HCN → NH ₃	Bose <i>et al.</i> , (1988)	X _{HCN} X _{OH}	parameters are coal dependent	
	Mitchell and Tarbell (1982)	X _{HCN} X _{O₂}	1.94x10 ¹⁴	78,500
NH ₃ → NO	de Soëte (1975)	X _{NH₃} X ^b _{O₂}	4.00x10 ⁶	32,000
	Mitchell and Tarbell (1982)	X _{NH₃} X _{O₂}	refer to Eq'n 15	
NH ₃ + NO → N ₂	de Soëte (1975)	X _{NH₃} X _{NO}	1.80x10 ⁸	27,000
	Bose <i>et al.</i> (1988)	X _{NH₃} X _{NO}	1.92x10 ⁴	22,500
	Mitchell and Tarbell (1982)	X _{NH₃} X _{NO}	6.22x10 ¹⁴	55,000

[‡] Rate parameters are from Miller and Bowman (1989) and Bowman (1975).

[§] The power for oxygen concentrations is determined from and auto correlation, $b = f(O_2)$, given by de Soëte (1975).

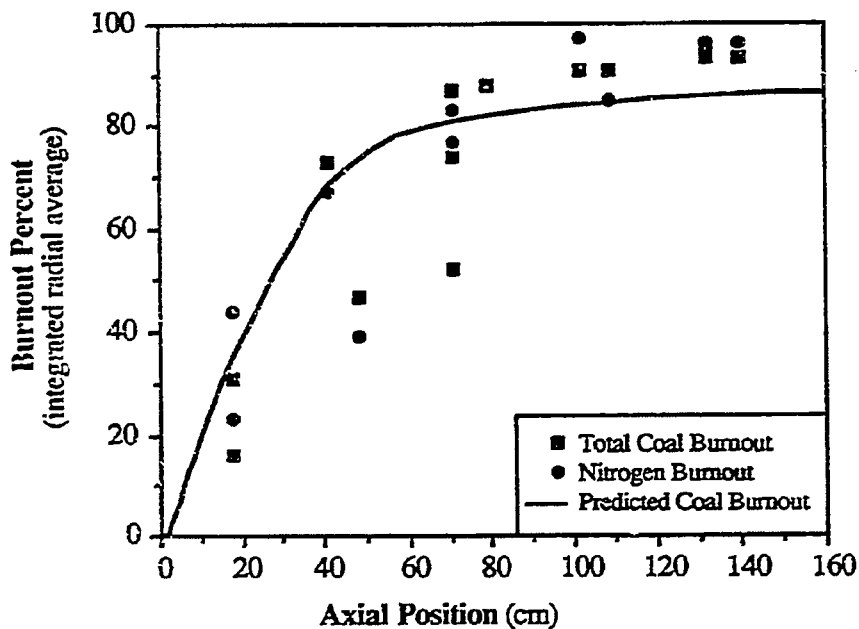


Fig. II.G-2. Wyoming subbituminous coal burnout. Experimental data are from Asay, (1982).

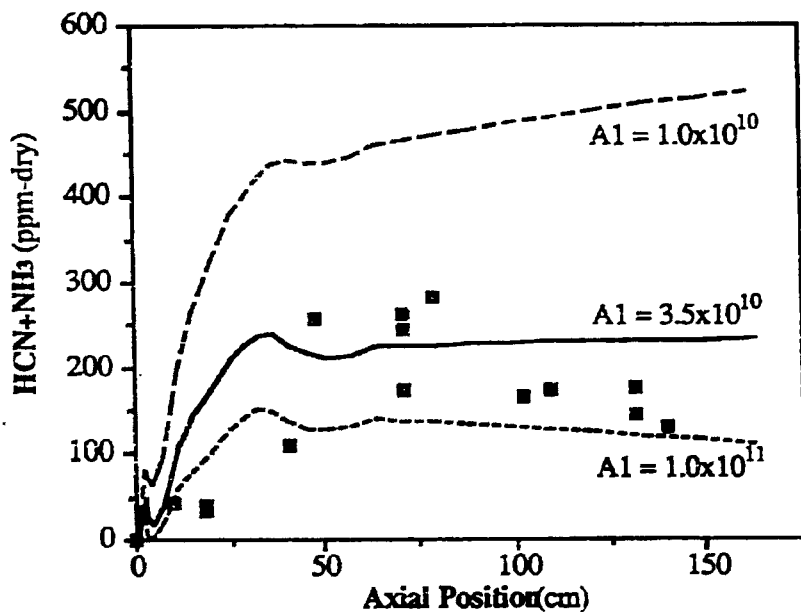
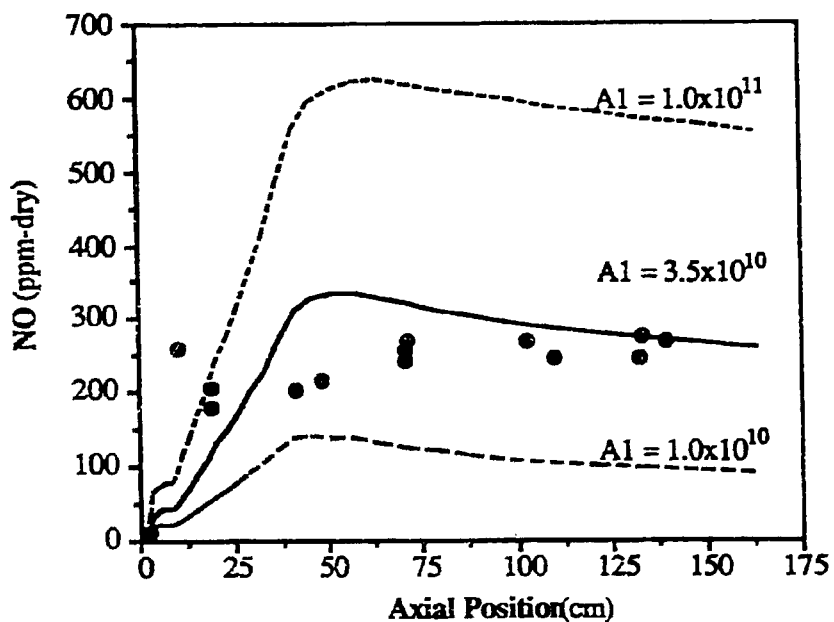


Fig.II.G-3. Comparison between predicted (curves) and measured (symbols) nitrogen integrated profile data for Wyoming subbituminous coal combustion. Different values of pre-exponential factor are for global conversion of HCN to NO. Data are from Asay (1982).

Mitchell and Tarbell suggest a value of $b=8$ with m being calculated from the coal ultimate analysis.

In the current evaluation study, the concentration of hydrocarbon fragments was related to the local amount of coal off-gas material. This approach gives spurious concentrations since coal off-gas material is rapidly oxidized as soon as the volatiles and oxidizer are mixed and is not continuously available for reaction with NO.

The comparisons with experimental data are plotted in Figure II.G-4. Calculated NO centerline concentrations rise above the measured data but then decay and drop below the aft-combustor measurements. The decrease in NO is a result of overpredicting the recycle reaction by assuming all coal off-gas material can react with NO. As NO concentrations diminish, HCN concentrations rise above the measured data. NH₃ concentrations are always predicted below measurements due to the significantly lower activation energy with respect to HCN and NO reactions. This may be considered the most serious limitation of the global kinetic of Mitchell and Tarbell (1982).

Predictions with the global kinetics reported by Wendt and coworkers (Bose et al, 1988) show somewhat better agreement with the measured NO concentrations (see Fig. II.G-5). However, the predicted HCN concentrations are far above the experimental data while the predicted NH₃ concentrations do not match the measurements aft in the reactor. This is due to low prediction of OH concentrations by PCGC-2. Wendt et al. (1989) presented an equation for estimating the "overshoot" in radical OH concentrations as a function of temperature:

$$OH = OH_{eq} \left[1.1 \times 10^{-4} \exp\left(\frac{15469}{T}\right) \right] \quad (II.G-2)$$

Using this expression to adjust the predicted equilibrium OH concentrations, the comparison between HCN and NH₃ profiles was improved. Because the expression given by Wendt et al. (1989) was correlated for their reactor conditions (which were fuel-rich), this expression is not recommended for all systems. However, the improved results obtained by employing this expression demonstrate that favorable predictions can be achieved when OH concentrations can be adequately predicted.

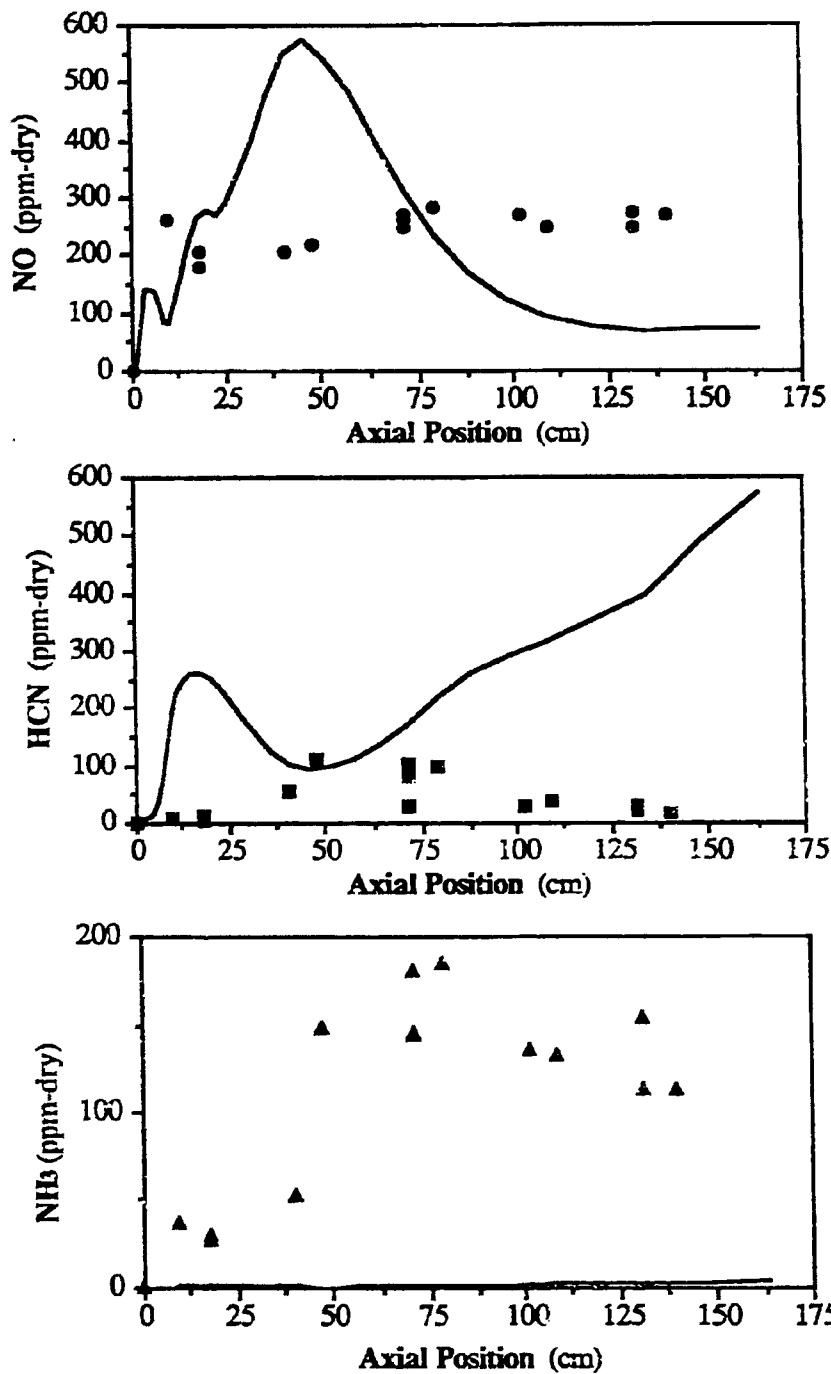


Fig.II.G-4. Comparison between predicted and measured nitrogen pollutant centerline profiles for Wyoming subbituminous coal using the alternative fuel NO mechanism with the empirical rates of Mitchell and Tarbell (1982). Data are from Asay (1982).

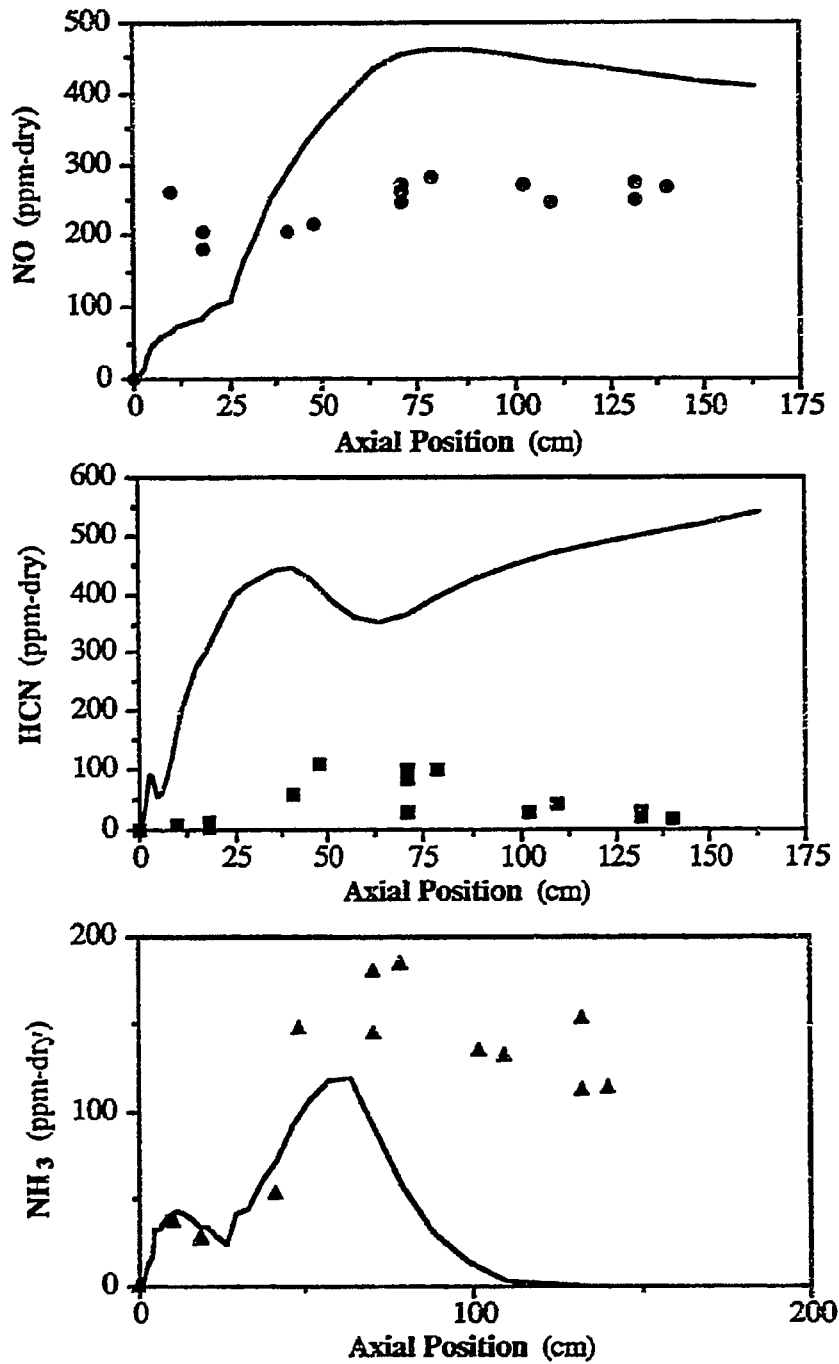


Fig. II.G-5. Comparison between predicted and measured nitrogen pollutant centerline profiles for Wyoming subbituminous coal using the alternative fuel NO mechanism with the global rate correlations reported by Bose et al., (1988). Data are from Asay (1982).

North Dakota Lignite Gasification - One of the primary objectives of this work was to investigate nitrogen conversion pathways during fuel-rich lignite coal combustion. Experimental evidence suggest that low-rank coal nitrogen is released as light gas NH_3 or is quickly converted from HCN to NH_3 in the vicinity of the coal particle (Chen et al., 1982). The observation of high NH_3 concentrations during low-rank coal processes provides the impetus for incorporating global reactions involving NH_3 into the model. The improved NO model allows nitrogen released from the coal and char to be partitioned between light gas HCN and NH_3 . The amount of total nitrogen assumed to be released as HCN is specified by the product $(\alpha_n \cdot \text{bcn})$ - where bcn is the percent of nitrogen in the coal. The remainder of volatile nitrogen, $(1 - \alpha_n) \cdot \text{bcn}$, is assumed to be instantaneously converted to NH_3 .

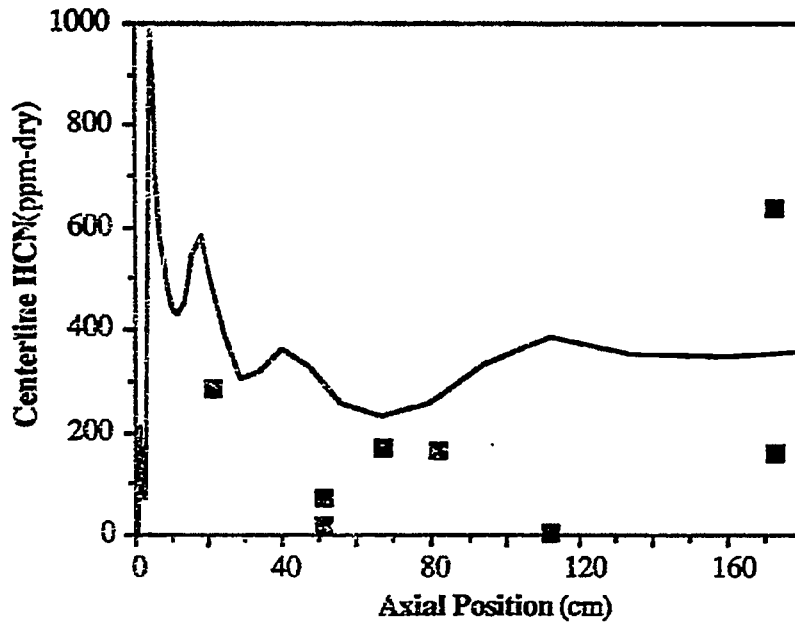
Experimental evidence also suggests that early coal volatiles during coal gasification are essentially nitrogen-free (Pohl and Sarofim, 1977; and Haussmann et al., 1988). A simple expression which relates nitrogen loss to coal off-gas mixture fraction was used to delay nitrogen release for the lignite case.

Figure II.G-6 shows that favorable agreement between predicted and measured HCN and NH_3 profiles when fuel nitrogen release was delayed until 20 percent of the total coal mass loss had occurred and was equally partitioned between HCN and NH_3 . The comparison between measured and predicted NO still lacks quantitative agreement but is substantially improved over former predictions (Boardman, 1987). These results demonstrate the need for an advanced nitrogen devolatilization model which includes an adequate description of light gas nitrogen devolatilization and species production depending on coal type.

Figure II.G-7 shows the NO centerline profile that was predicted for gasification of North Dakota lignite using the global kinetics of Wendt and coworkers (Bose et al., 1988). The lower curve was obtained by assuming half of the volatile nitrogen is released as NH_3 . Although the profiles vary significantly from the reported data, they are similar to the predictions made with the revised fuel NO mechanism.

The empirical kinetics of Mitchell and Tarbell (1982) did not match any of the nitrogen-containing pollutant profiles for this case.

a.Centerline HCN profiles



b.Centerline NH₃ profiles

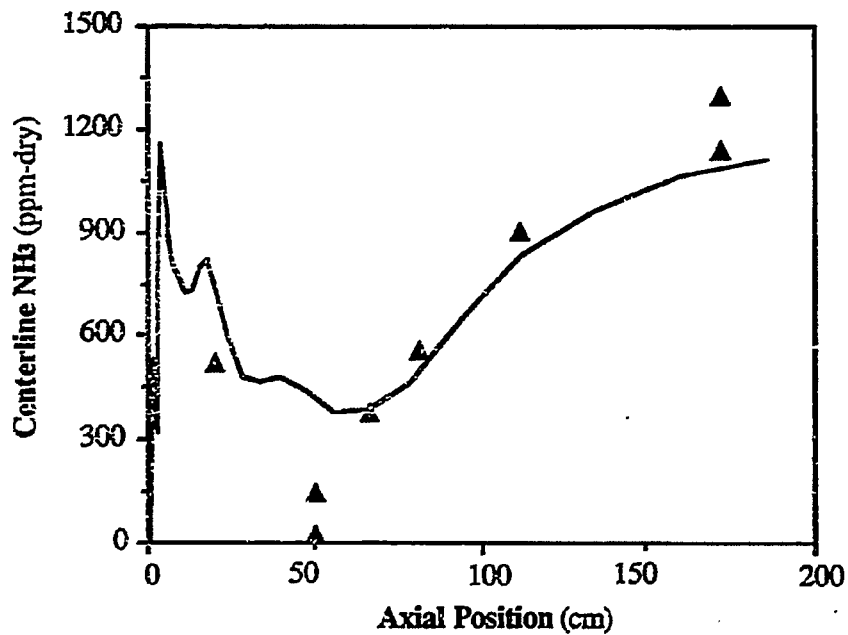


Figure II.G-6. Comparison between predicted and measured NO centerline profiles with delayed release of volatile North Dakota lignite nitrogen and equal partitioning between HCN and NH₃. Data are from Brown (1985).

c.Centerline NO profiles

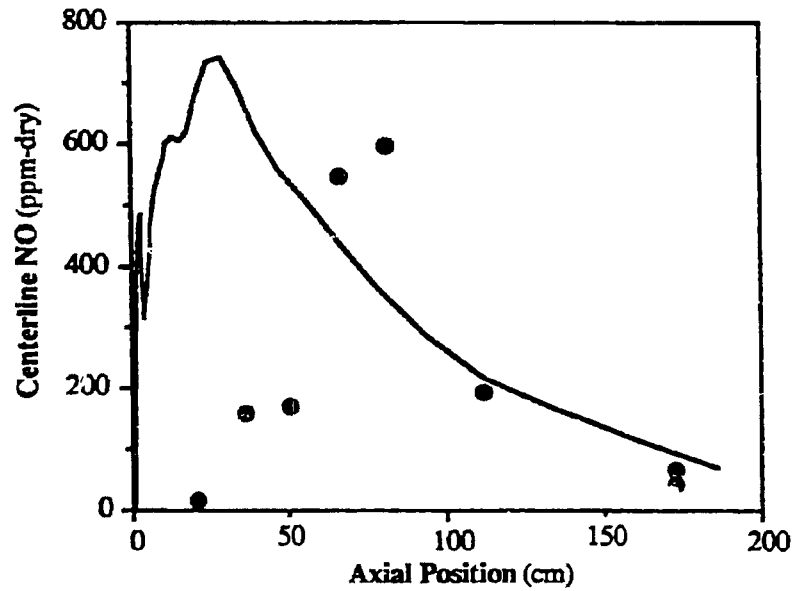


Figure II.G-6 (cont'd). Comparison between predicted and measured NO centerline profiles with delayed release of volatile North Dakota lignite nitrogen and equal partitioning between HCN and NH_3 . Data are from Brown (1985).

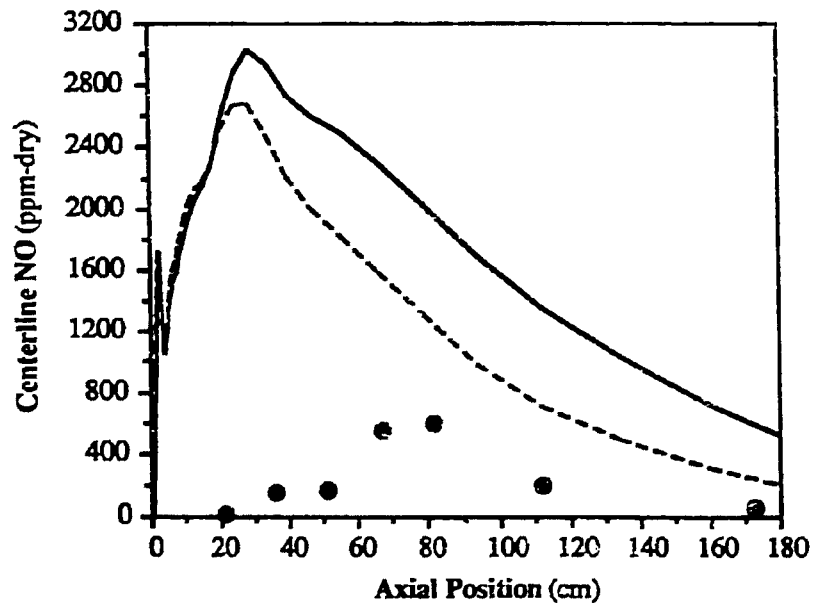


Fig.II.G-7. Comparison between predicted and measured nitrogen pollutant centerline profiles for North Dakota lignite gasification using the alternative fuel NO mechanism with the global rate correlation of Bose et al., (1988). Upper curve assumes all coal nitrogen is released as HCN. Lower curve assumes 50 percent of coal nitrogen is released as NH_3 . Data are from Brown (1985).

NO_x concentrations exceeding 8000 ppm were predicted in the proximity of the burner for the North Dakota lignite case. These concentrations rapidly decayed to negligible quantities.

Summary of Fuel NO Mechanisms Evaluations

The results of this study show that NO concentrations can be viably predicted using the improved fuel NO mechanism (Figure II.G-1a). The lignite gasification case was more favorably predicted when nitrogen release rate was delayed and nitrogen volatiles were partitioned between HCN and NH₃. Based on the model predictions, NH₃ appears to be important in the early volatile products.

The alternative fuel NO mechanism gave mixed results. The global kinetic expression reported by Bose et al. (1988) appears to give favorable predictions if OH concentrations can be correctly estimated. Predictions with the kinetics of Mitchell and Tarbell (1982) did not successfully match nitrogen pollutant profiles for either combustion or gasification cases.

Until methods or models are available to predict OH concentrations, the improved fuel NO mechanism (Figure II.G-1a) appears to be the most reliable choice for predicting fuel NO formation during pulverized coal combustion and gasification. If OH concentrations can be estimated, the alternative fuel-NO mechanism (Figure II.G-1b) would provide a useful method for predicting NO concentrations, thus increasing the power of the NO model as a design tool.

Joint Thermal and Fuel NO Predictions

Thermal NO Formation During Coal Combustion - When the thermal NO mechanism was jointly solved with the fuel NO mechanism, the impact on total NO concentrations was less than the sum of the individual mechanisms. Thermal NO concentrations in excess of 25 ppm were predicted for the Wyoming subbituminous cases when the fuel NO mechanism was not included in the calculations. An incremental difference of less than 10 ppm NO was predicted when the thermal NO and fuel NO were jointly predicted (see Figure II.G-8). The primary reason for this result is the decay of thermal NO by fuel nitrogen intermediates but also includes competition for oxygen concentrations. This finding matches the observation of Pershing and Wendt (1976) who showed that thermal NO concentrations in their laboratory-scale combustor were less than 5 percent at reactor temperatures below 2200 K.

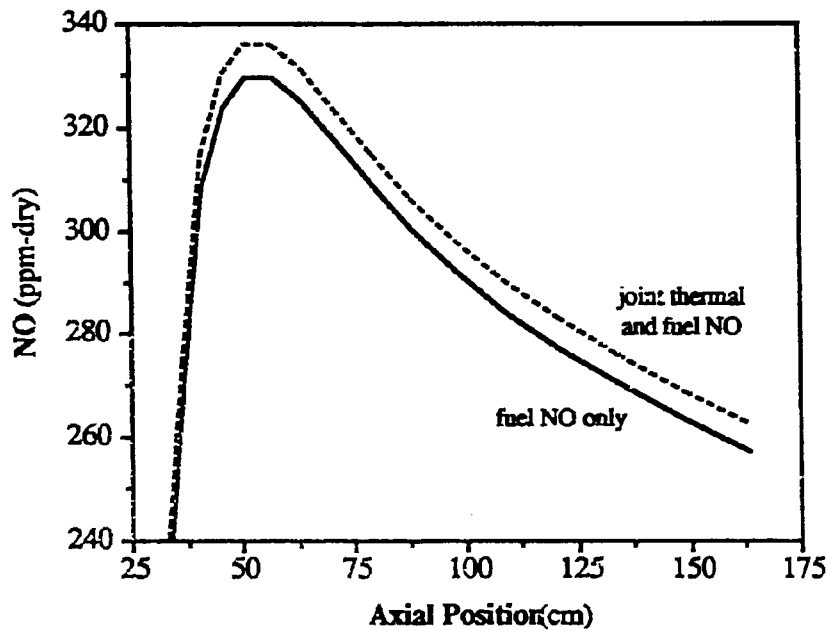


Figure II.G-8. Joint thermal and fuel NO mechanism prediction of NO concentrations for Wyoming coal combustion case. Thermal NO calculations assume radical oxygen concentrations are in quasi-equilibrium with molecular oxygen

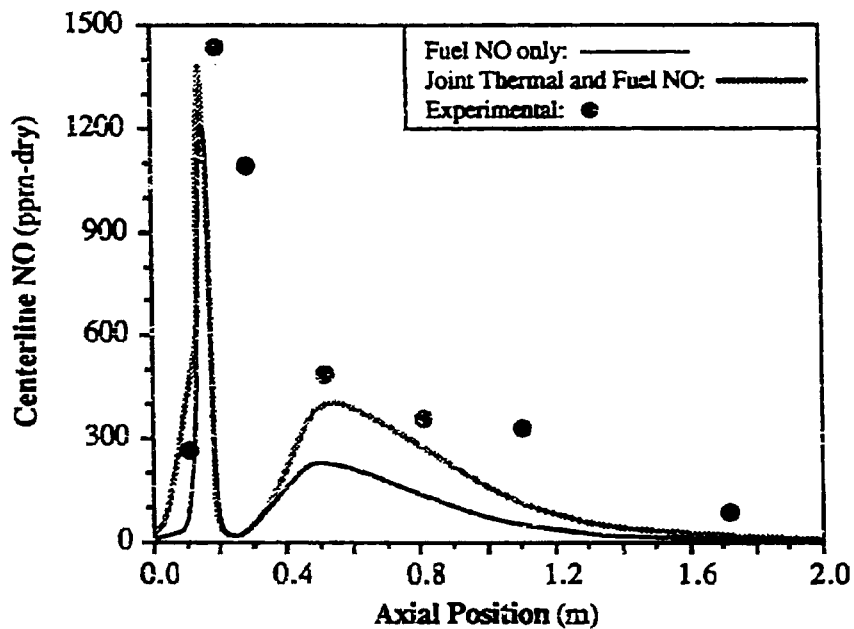


Figure II.G-9. Comparison between measured and predicted NO centerline concentrations for gasification of Utah bituminous coal at 1 atm. Predicted curves made with and without the thermal NO mechanism included in the calculation. Data are from Brown (1985).

The value of separately predicting fuel and thermal NO contributions is the power to identify appropriate NO_x abatement strategies. For instance, thermal NO may or may not be significant when over-fire air registers are employed in a combustor. If thermal NO is found to be important in the staging air, then strategic placement of the air registers could reduce total NO emissions.

Thermal NO Formation During Coal Gasification - The potential for thermal NO formation is reduced in the absence of oxidizing air and purge nitrogen. In order for thermal NO to form, N₂ must first build up as a result of fuel nitrogen decay. Even when all of the nitrogen in the coal is converted to gaseous N₂, the predicted amount of thermal NO formed was only a few ppm during North Dakota lignite gasification. The addition of window purge nitrogen, however, can lead to appreciable thermal NO formation. Figure II.G-9 shows the relative contribution of thermal NO during the gasification of Utah bituminous coal when a small amount of purge nitrogen (< 10 mole percent) was added to the secondary stream inlet. The predicted incremental contribution of thermal NO is 20% where the NO concentration is maximum. In the aft section of the gasifier, thermal NO brings the predicted profile up to the level of the measured data. Hence, the inclusion of the thermal NO mechanism into the model substantially improved the agreement between predicted and measured NO values when nitrogen was included in the inlet feed.

NO Submodel User Guidelines

User instructions for running the revised NO submodel have been written (Boardman, 1990). In this document, a description of the input flags which govern the optional mechanisms and rate expression that are used to calculate NO formation and destruction is given. The logical sequencing of the code is discussed. A discussion about convergence parameters is also provided to aid users in achieving converged solutions.

SO_x-Sorbent Particle Reaction Submodel

Tracking the Sorbent Particles - Work was initiated under Subtask 3.c to modify PCGC-2 to track reacting sorbent particles and account for their effects on the gas.

Sulfur/Sorbent Reaction - Sorbent capture of sulfur species will be predicted using a simplified version of the grain model of Silcox (1985). This model accounts for diffusion of reactants through the porous structure of the particle, diffusion through the product CaSO_4 , and reaction at the CaO-CaSO_4 interface. The grains are assumed to react by the shrinking core model. The reaction rate of SO_2 and H_2S will be correlated to experimental data available in the open literature. The governing equation for Silcox's model is a partial differential equation to determine the concentration profile in a sorbent particle. Thus, the solution of the model is not trivial and will require the development of an efficient subroutine and solver. Gaseous SO_2 and H_2S concentrations will be determined by solving species continuity for each species.

SO_x -Sorbent Reaction Submodel Evaluation - Prediction of gaseous sulfur species has been presented in previous quarterly reports. In addition to these cases, the data measured in the BYU gasifier by Huber (1989) under Subtask 2.h will be used to evaluate the SO_x -sorbent reaction submodel.

Plans

Work on the sorbent reactions submodel will continue.